

Optimal analysis of the CMB trispectrum

Kendrick M. Smith,¹ Leonardo Senatore,^{2,3} and Matias Zaldarriaga⁴

¹*Perimeter Institute for Theoretical Physics, Waterloo, ON N2L 2Y5, Canada*

²*Stanford Institute for Theoretical Physics, Stanford University, Stanford, CA 94305, USA*

³*Kavli Institute for Particle Astrophysics and Cosmology,*

SLAC and Stanford University, Menlo Park, CA 94025, USA

⁴*Institute for Advanced Study, Einstein Drive, Princeton, NJ 08540, USA*

(Dated: November 6, 2018)

We develop a general framework for data analysis and phenomenology of the CMB four-point function or trispectrum. To lowest order in the derivative expansion, the inflationary action admits three quartic operators consistent with symmetry: $\dot{\sigma}^4$, $\dot{\sigma}^2(\partial\sigma^2)$, and $(\partial\sigma)^4$. In single field inflation, only the first of these operators can be the leading non-Gaussian signal. A Fisher matrix analysis shows that there is one near-degeneracy among the three CMB trispectra, so we parameterize the trispectrum with two coefficients $g_{NL}^{\dot{\sigma}^4}$ and $g_{NL}^{(\partial\sigma)^4}$, in addition to the coefficient g_{NL}^{loc} of ζ^3 -type local non-Gaussianity. This three-parameter space is analogous to the parameter space $(f_{NL}^{\text{loc}}, f_{NL}^{\text{eq}}, f_{NL}^{\text{orth}})$ commonly used to parameterize the CMB three-point function. We next turn to data analysis and show how to represent these trispectra in a factorizable form which leads to computationally fast operations such as evaluating a CMB estimator or simulating a non-Gaussian CMB. We discuss practical issues in CMB analysis pipelines, and perform an optimal analysis of WMAP data. Our minimum-variance estimates are $g_{NL}^{\text{loc}} = (-3.80 \pm 2.19) \times 10^5$, $g_{NL}^{\dot{\sigma}^4} = (-3.20 \pm 3.09) \times 10^6$, and $g_{NL}^{(\partial\sigma)^4} = (-10.8 \pm 6.33) \times 10^5$ after correcting for the effects of CMB lensing. No evidence of a nonzero inflationary four-point function is seen.

I. INTRODUCTION AND MAIN RESULTS

Uncovering the nature of inflation is one of the most important open questions in our current cosmological model. Non-Gaussianity of the primordial density perturbations probes the interaction structure of the inflationary Lagrangian. Since interactions contain most of the information on the dynamics of the fields, the search for primordial non-Gaussianity has played a central role in constraining the physics of inflation.

So far, the search for non-Gaussianity has been focused mainly on the bispectrum, or 3-point function. Limits on the inflationary 3-point function have been obtained following two different approaches. The first is based on providing templates for 3-point functions that are matched against the data, while the second approach attempts to reconstruct a generic 3-point function from the data. The first method has the advantage that it can be restricted to theoretically motivated models over which one can perform an optimal analysis, but the disadvantage of potentially missing a signal in the data simply because it was not looked for. It has been used to search for the (now) well-known local [1–4], equilateral [5], and orthogonal [6] template bispectra, plus some very recently identified higher-derivative bispectra [7]. The second approach (e.g. [8]) has the advantage of being sensitive to any potential signal, but the disadvantage that significance of a signal can be diluted away as many independent shapes are matched to the data.

At present, the most constraining search for non-Gaussianity is provided by Planck [9], which finds no evidence of non-Gaussianity. While this analysis is a huge observational achievement, it should be stressed that from a particle physics point of view the limit is still rather weak. The skewness of the distribution of the primordial fluctuations is constrained to be smaller than about 10^{-3} . This constrains inflation to be more or less as interacting as the electron in quantum electrodynamics, or as the pion at energies of order of its mass. It would be clearly very interesting to further constrain the level of non-Gaussianity by one or two orders of magnitude, a sensitivity that the recently developed effective field theory of large scale structure [10] has shown the potential to achieve with surveys in the next decade.

The observational interest in non-Gaussianity is not just due to the fact that it is related to the dynamics of the theory. It additionally represents a very non-trivial signal. Because of translation and rotation invariance, the two point function of the primordial density perturbation is described by a scalar function of the modulus of the wavenumber k . Once we impose approximate scale invariance, this function can be described by a number, the amplitude, and another number, the slight deviation from scale invariance, the tilt. Instead, after assuming the same symmetries (*i.e.* translation, rotation and scale invariance), the bispectrum is described by a scalar function of two scalar variables [11]. We pass from one single number to a full function of two variables. Clearly, a detection of such a signal would be an extremely non-trivial signature in the sky. It is the same information that describes 2-to-2 scattering in a collider. When we pass to the trispectrum, the same symmetries make the trispectrum a scalar function of five variables. This is a fantastically non-trivial function that if we were so lucky to be able to see it in the sky, it

would offer tremendous constraining power on the physics of inflation.

The analysis of the trispectrum, or four-point function, of the primordial density perturbation is less developed than the bispectrum. We briefly summarize existing results in the literature. The so-called g_{NL}^{loc} trispectrum is generated if the primordial curvature perturbation $\zeta(\vec{x})$ can be expressed in the form:

$$\zeta(\vec{x}) = \zeta_g(\vec{x}) + \frac{9}{25}g_{NL}^{\text{loc}}\zeta_g(\vec{x})^3 \quad (1)$$

where ζ_g is a Gaussian field. This leads to the following ζ -trispectrum:

$$\langle \zeta_{\mathbf{k}_1} \zeta_{\mathbf{k}_2} \zeta_{\mathbf{k}_3} \zeta_{\mathbf{k}_4} \rangle = \frac{54}{25}g_{NL}^{\text{loc}} \left(P_\zeta(k_1)P_\zeta(k_2)P_\zeta(k_3) + 3 \text{ perm.} \right) (2\pi)^3 \delta^3 \left(\sum \mathbf{k}_i \right) \quad (2)$$

While it is impossible to obtain such a signal in single field inflation, as Maldacena's consistency condition [12] generalized to the four-point function (e.g. [13]) shows ¹, there are technically natural multifield inflationary models that generate this signal without generating an observationally larger bispectrum [4]. If we call the additional light field σ 's, a measurable g_{NL}^{loc} can be enforced by imposing, just as an example, an approximate Z_2 symmetry of the σ 's or protecting them with an approximate supersymmetry [4]. Several groups have constrained g_{NL}^{loc} from WMAP data [15–18], and most recently [19] who use the optimal estimator.

Another ‘‘local’’ four-point function is the τ_{NL} -trispectrum, defined by:

$$\langle \zeta_{\mathbf{k}_1} \zeta_{\mathbf{k}_2} \zeta_{\mathbf{k}_3} \zeta_{\mathbf{k}_4} \rangle = \tau_{NL} P_\zeta(k_2)P_\zeta(k_4)P_\zeta(|\mathbf{k}_1 + \mathbf{k}_2|) (2\pi)^3 \delta^3 \left(\sum \mathbf{k}_i \right) + (11 \text{ perm.}) \quad (3)$$

The τ_{NL} -trispectrum can arise if ζ is a local quadratic combination of multiple uncorrelated fields. For example, suppose

$$\zeta(\mathbf{x}) = \zeta_G(\mathbf{x}) + A\zeta_G(\mathbf{x})\sigma(\mathbf{x}) \quad (4)$$

where A is a free parameter and ζ_G, σ are uncorrelated Gaussian fields with equal power spectra. In this model, the three-point function is zero and the four-point function takes the form (3) with $\tau_{NL} = A^2$. The parameter τ_{NL} has been constrained from WMAP [16, 18] and Planck [9] data.

Going beyond the local-type signals g_{NL}^{loc} and τ_{NL} , the only primordial trispectrum which has been constrained is an ‘‘equilateral’’ trispectrum, which we will denote $g_{NL}^{\dot{\sigma}^4}$ and define by:

$$\begin{aligned} \langle \zeta_{\mathbf{k}_1} \zeta_{\mathbf{k}_2} \zeta_{\mathbf{k}_3} \zeta_{\mathbf{k}_4} \rangle &= \frac{9216}{25}g_{NL}^{\dot{\sigma}^4} A_\zeta^3 \int_{-\infty}^0 d\tau_E \tau_E^4 \left(\prod_{i=1}^4 \frac{e^{k_i \tau_E}}{k_i} \right) (2\pi)^3 \delta^3 \left(\sum \mathbf{k}_i \right) \\ &= \frac{221184}{25}g_{NL}^{\dot{\sigma}^4} A_\zeta^3 \frac{1}{k_1 k_2 k_3 k_4 (k_1 + k_2 + k_3 + k_4)^5} (2\pi)^3 \delta^3 \left(\sum \mathbf{k}_i \right) \end{aligned} \quad (5)$$

where A_ζ is the amplitude of the ζ power spectrum, defined by $P_\zeta(k) = A_\zeta/k^3$. In the effective field theory description of inflation, this trispectrum arises from a quartic operator of the schematic form $\dot{\sigma}^4$ (we will be more precise in the next section). WMAP5 constraints on this trispectrum were reported in [17].

Now is a good time to explain our normalization convention in Eq. (5). Recall that in the bispectrum case, the bispectrum parameters ($f_{NL}^{\text{eq}}, f_{NL}^{\text{orth}}$) are normalized by fixing the bispectrum amplitude on equilateral triangles to have the same value as the local bispectrum with $f_{NL}^{\text{loc}} = 1$. Analogously, we normalize trispectra so that $\langle \zeta_{\mathbf{k}_1} \zeta_{\mathbf{k}_2} \zeta_{\mathbf{k}_3} \zeta_{\mathbf{k}_4} \rangle = (216/25)g_{NL}^{\text{loc}} A_\zeta^3/k^9$ for tetrahedral 4-point configurations with $|\mathbf{k}_i| = k$ and $\mathbf{k}_i \cdot \mathbf{k}_j = -k^2/3$ for $i \neq j$. This convention fixes all trispectra to have the same value on tetrahedrons as the local trispectrum with $g_{NL}^{\text{loc}} = 1$. Another detail: in Eq. (5), and in Eqs. (6), (7) below, we write the trispectrum in two forms, either with a time integral which is unevaluated, or after evaluation of the integral. We do this because the first form will be directly useful when obtaining factorizable representations for the trispectra, as we will explain later.

¹ The fact that Maldacena's consistency condition gives a non-zero bispectrum or trispectrum in the squeezed limit should not be regarded as predicting a non-vanishing physical signal in that limit. It is indeed the way to write in comoving coordinates the fact that there is no physical correlation among modes of different wavelengths: a local observer can obtain the same result for a local experiment by starting with vanishing super-Hubble correlations. See discussion about this in [14].

In this paper, we will introduce two new trispectrum shapes which correspond to quartic operators of the form $\dot{\sigma}^2(\partial_i\sigma)^2$ and $(\partial_i\sigma)^2(\partial_j\sigma)^2$ in the effective field theory of inflation. Following our normalization convention above, we define parameters $g_{NL}^{\dot{\sigma}^2(\partial\sigma)^2}$ and $g_{NL}^{(\partial\sigma)^4}$ by:

$$\begin{aligned} \langle \zeta_{\mathbf{k}_1} \zeta_{\mathbf{k}_2} \zeta_{\mathbf{k}_3} \zeta_{\mathbf{k}_4} \rangle &= -\frac{13824}{325} g_{NL}^{\dot{\sigma}^2(\partial\sigma)^2} A_\zeta^3 \int_{-\infty}^0 d\tau_E \tau_E^2 \left(\frac{(1-k_3\tau_E)(1-k_4\tau_E)}{k_1 k_2 k_3^3 k_4^3} (\mathbf{k}_3 \cdot \mathbf{k}_4) e^{\sum k_i \tau_E} + (5 \text{ perm.}) \right) \\ &\quad \times (2\pi)^3 \delta^3 \left(\sum \mathbf{k}_i \right) \\ &= -\frac{27648}{325} g_{NL}^{\dot{\sigma}^2(\partial\sigma)^2} A_\zeta^3 \left(\frac{K^2 + 3(k_3 + k_4)K + 12k_3 k_4}{k_1 k_2 k_3^3 k_4^3 K^5} (\mathbf{k}_3 \cdot \mathbf{k}_4) + 5 \text{ perm.} \right) (2\pi)^3 \delta^3 \left(\sum \mathbf{k}_i \right) \end{aligned} \quad (6)$$

$$\begin{aligned} \langle \zeta_{\mathbf{k}_1} \zeta_{\mathbf{k}_2} \zeta_{\mathbf{k}_3} \zeta_{\mathbf{k}_4} \rangle &= \frac{82944}{2575} g_{NL}^{(\partial\sigma)^4} A_\zeta^3 \int_{-\infty}^0 d\tau_E \left(\prod_{i=1}^4 \frac{(1-k_i\tau_E) e^{k_i\tau_E}}{k_i^3} \right) \left((\mathbf{k}_1 \cdot \mathbf{k}_2)(\mathbf{k}_3 \cdot \mathbf{k}_4) + (2 \text{ perm.}) \right) (2\pi)^3 \delta^3 \left(\sum \mathbf{k}_i \right) \\ &= \frac{165888}{2575} g_{NL}^{(\partial\sigma)^4} A_\zeta^3 \left(\frac{2K^4 - 2K^2 \sum k_i^2 + K \sum k_i^3 + 12k_1 k_2 k_3 k_4}{k_1^3 k_2^3 k_3^3 k_4^3 K^5} \right) \\ &\quad \times \left((\mathbf{k}_1 \cdot \mathbf{k}_2)(\mathbf{k}_3 \cdot \mathbf{k}_4) + (2 \text{ perm.}) \right) (2\pi)^3 \delta^3 \left(\sum \mathbf{k}_i \right) \end{aligned} \quad (7)$$

where $K = k_1 + k_2 + k_3 + k_4$. In this paper, we will implement the optimal CMB estimator for four trispectra: g_{NL}^{loc} , $g_{NL}^{\dot{\sigma}^4}$, $g_{NL}^{\dot{\sigma}^2(\partial\sigma)^2}$, and $g_{NL}^{(\partial\sigma)^4}$. (The τ_{NL} trispectrum requires slightly different techniques for reasons that will be apparent later, so we have omitted it in this paper.) Searching for these four trispectra is analogous to searching for the standard bispectra f_{NL}^{loc} , f_{NL}^{eq} , and f_{NL}^{orth} .²

There is a basic computational problem which arises for computational operations with trispectra, for example applying an estimator to CMB maps, or computing a Fisher matrix. Naively, these operations have computational cost $\mathcal{O}(\ell_{\text{max}}^7)$, which is prohibitive for a large experiment like WMAP or Planck with $\ell_{\text{max}} \sim 10^3$. The same computational problem arises for the bispectrum, where it has been solved using the idea of *factorizability* [3, 5, 8, 20–22]. If a bispectrum can be represented as a sum of terms which satisfy a suitable factorizability condition (the precise condition is given in Eq. (38) below), then computational cost is dramatically reduced. A variety of general strategies have been proposed for making bispectrum data analysis computationally feasible (e.g. [8, 21–24]); while the details of these proposals are very different, they can all be viewed as different strategies for representing a bispectrum as a sum of factorizable terms. Analogously for the trispectrum, we will formulate a suitable definition of factorizability, show that it leads to dramatically reduced computational cost, and give a physically motivated, Feynman diagram based prescription for representing inflationary trispectra in factorizable form. This will allow us to analyze the local, $\dot{\sigma}^4$, $\dot{\sigma}^2(\partial\sigma)^2$, and $(\partial\sigma)^4$ trispectra.

Among other things, factorizability means that we can do a Fisher matrix analysis of correlations between trispectra. We will show that there is one near-degeneracy among the four trispectra. To quantify this, the $\dot{\sigma}^2(\partial\sigma)^2$ trispectrum is 99.2% correlated with a suitably chosen linear combination of the $\dot{\sigma}^4$ and $(\partial\sigma)^4$ trispectra. Therefore, we will eliminate the parameter $g_{NL}^{\dot{\sigma}^2(\partial\sigma)^2}$, and reduce our set of trispectra to three: g_{NL}^{loc} , $g_{NL}^{\dot{\sigma}^4}$, and $g_{NL}^{(\partial\sigma)^4}$.

We will construct trispectrum estimators and present details of analysis pipelines which are suitable for realistic experiments such as WMAP or Planck. We would like to emphasize three technical issues from the outset.

First, the trispectrum estimator is potentially very sensitive to modeling errors in the two-point function due to slightly incorrect cosmological parameters, detector noise properties, or beams. Suppose the trispectrum is estimated assuming covariance matrix C_0 , but the true covariance is $C_{\text{true}} = C_0 + \Delta C$. The trispectrum estimators we use will have the property that the resulting bias is parametrically $\mathcal{O}((\Delta C)^2)$ rather than $\mathcal{O}(\Delta C)$. This property turns out to be critical in practice.

The second issue is that many technical tricks are necessary to reduce the number of Monte Carlo simulations in the trispectrum estimation pipeline to a reasonable level. We will find several situations where an “obvious” Monte Carlo procedure is slow, but there is an alternate Monte Carlo procedure which is faster (examples include Eqs. (66), (83), and (F2)).

Third, gravitational lensing and other secondary effects (such as contamination by residual infrared sources) generate a nonzero trispectrum which must be subtracted. The lensing trispectrum has been measured in ACT [25, 26], SPT [27, 28], and Planck [29], with recent measurements approaching 40σ ! Although lensing is an interesting source

² Recall that the space of bispectra spanned by f_{NL}^{eq} , f_{NL}^{orth} is equal, by a linear transformation, to the space generated by the cubic operators $\dot{\sigma}^3$ and $\dot{\sigma}(\partial\sigma)^2$ [6].

of cosmological information, in this paper our focus will be on the primordial trispectrum, so we will treat lensing as a large contaminant whose bias must be subtracted when estimating other trispectrum shapes.

We will conclude by performing an optimal analysis of WMAP data. We find the following constraints (all 95% CL):

$$\begin{aligned} (-8.18 \times 10^5) &< g_{NL}^{\text{loc}} < (0.58 \times 10^5) \\ (-9.38 \times 10^6) &< g_{NL}^{\dot{\sigma}^4} < (2.98 \times 10^6) \\ (-2.34 \times 10^6) &< g_{NL}^{(\partial\sigma)^4} < (0.19 \times 10^6) \end{aligned} \quad (8)$$

We find no evidence of primordial trispectra, and the error bars agree with Fisher matrix forecasts.

II. MINI-REVIEW OF EFFECTIVE FIELD THEORIES OF SINGLE AND MULTIFIELD INFLATION

In this section we briefly review the particle physics motivation for studying the trispectra that we analyze. We do this by using the effective field theory of inflation [30] and of multifield inflation [4].

We start from single field inflation. By assuming that inflation is an early phase of the universe characterized by a spontaneous breaking of time diffeomorphisms, it is possible to construct a model independent Lagrangian for the fluctuations. Furthermore, in inflation we are interested in computing correlation functions at an energy scale around the Hubble scale during the early quasi de Sitter phase. Often, this energy scale is high enough to write the action in the so-called decoupling limit, where the Lagrangian takes a very simple form:

$$\begin{aligned} S_\pi = \int d^4x \sqrt{-g} \left[-M_{\text{Pl}}^2 \dot{H} (\partial_\mu \pi)^2 + 2M_2^4 \left(\dot{\pi}^2 + \dot{\pi}^3 - \dot{\pi} \frac{(\partial_i \pi)^2}{a^2} + (\partial_\mu \pi)^2 (\partial_\nu \pi)^2 \right) \right. \\ \left. - \frac{M_3^4}{3!} (8 \dot{\pi}^3 + 12 \dot{\pi}^2 (\partial_\mu \pi)^2 + \dots) + \frac{M_4^4}{4!} (16 \dot{\pi}^4 + 32 \dot{\pi}^3 (\partial_\mu \pi)^2 + \dots) + \dots \right]. \end{aligned} \quad (9)$$

where ‘ \dots ’ represents higher order terms, higher derivative terms, and slow-roll suppressed terms. Here spatial indexes i are contracted with the δ^{ij} -tensor, while space-time indexes μ are contracted with the FRW metric $g^{\mu\nu}$. The field π represents the Goldstone boson of time translations. It is related to the curvature perturbation ζ as

$$\zeta = -H\pi + (\text{higher-order terms}). \quad (10)$$

The non-linear realization of time-diffeomorphisms forces the appearance of π into non-linear blocks. Simple inspection of the action shows that it is impossible to have a four-point function induced by operators of the form $\dot{\pi}^2 (\partial_\mu \pi)^2$ and $(\partial_\mu \pi)^2 (\partial_\nu \pi)^2$ that is the leading non-Gaussian signal: when these operators are turned on, there is always a cubic operator that induces a bispectrum with much higher signal-to-noise ratio [31]. At the level of the leading derivative operators, the only term that has a chance of producing a trispectrum without a bispectrum with a large signal-to-noise ratio is the operator $\dot{\pi}^4$. One should be careful about radiative corrections though. The non-linear realization of time-diffeomorphisms forces the presence of a quintic operator $\dot{\pi}^3 (\partial_\mu \pi)^2$ together with $\dot{\pi}^4$. One is naturally lead to wonder if this operator will induce, under radiative corrections, a cubic operator that dominates the signal. It turns out that the relative coefficients of $\dot{\pi}^4$ and $\dot{\pi}^3 (\partial_\mu \pi)^2$ are fixed by time-diffeomorphism invariance in such a way that, when the signal-to-noise in $\dot{\pi}^4$ is large ($g_{NL}^{\dot{\pi}^4} \gg 10^5$), the radiative corrections induced by the quintic operator generate at most a cubic operator $\dot{\pi}^3$ and $\dot{\pi} (\partial_\mu \pi)^2$ with an $f_{NL} \sim 1$, and therefore subleading [31]. This can be interpreted as an approximate Z_2 symmetry of the inflaton.³ We therefore conclude that it is possible to have a trispectrum induced by $\dot{\pi}^4$ as the leading non-Gaussian signal. A constraint on this trispectrum can be directly mapped, in the context of single field inflation, into a constraint of the coefficient M_4^4 of (9), as already done by the WMAP and the Planck experiments for the coefficients M_2^4 and M_3^4 from analysis of f_{NL}^{equil} and f_{NL}^{orthog} [6, 9, 34].

It is also possible to have higher derivative interactions leading to large non-Gaussianities directly in the form of a trispectrum from interactions with more than four overall derivatives, very schematically of the form $(\partial^2 \pi)^4$ [7, 31, 35–38]. As for the case of the three-point function, where the same phenomenon appears, the signal can be made detectable

³ The fact that the coefficient of $\dot{\pi}^4$ is unrelated to the coefficients of the cubic terms had been already noticed in [32, 33] for a subclass of the models we consider with the effective field theory consisting of scalar field Lagrangians of the form $P((\partial\phi)^2, \phi)$. However, without the identification of a mechanism protecting the generation of cubic terms, it is hard to imagine why one should concentrate on the particular Lagrangian allowing for a large quartic operator and small cubic ones.

only by lowering enough the unitarity bound of the theory, and it is furthermore possible to have strong degeneracies with shapes with fewer derivatives. This makes the prospects of detection somewhat more unlikely. We leave the study of these shapes to future work.

We now pass to multifield inflation. An effective field theory description of multifield inflation can be constructed after realizing that the predictions of multifield inflation largely do not depend on the background solution, with scalar fields developing possibly complicated trajectories in field space, but simply on the Lagrangian of the fluctuations. This Lagrangian can be simply constructed by coupling additional light degrees of freedom to the Goldstone boson of time-translations π . The main difference between single field and multifield inflation is that while in single field inflation the relationship between the Goldstone boson π and the curvature perturbation ζ is fixed by the background cosmology as in Eq. (10), the same is not true for the effect of the additional inflationary fields on ζ . How much a given fluctuation of the additional fields contributes to the curvature perturbations depends on the whole trajectory of the fields from the time a mode crosses the horizon to reheating, and also on the details of the reheating epoch. However, the fact that these effects happen when all the modes of interest are outside of the horizon and gradients are therefore negligible (see Fig. 1) permits a crucial simplification [4]: the relationship between the fluctuations of additional scalar fields, σ_I , and ζ , must be local in space, and since fluctuations are quasi-Gaussian, the relationship can be Taylor expanded. We are therefore led to

$$\begin{aligned} \zeta(x) = & -H \pi(x) + \left(\frac{\partial \zeta}{\partial \sigma_I} \right)_0 \sigma_I(x) + \left(\frac{\partial^2 \zeta}{\partial \pi \partial \sigma_I} \right)_0 \pi(x) \sigma_I(x) + \frac{1}{2!} \left(\frac{\partial^2 \zeta}{\partial \sigma_I \partial \sigma_J} \right)_0 \sigma_I(x) \sigma_J(x) \\ & + \frac{1}{3!} \left(\frac{\partial^3 \zeta}{\partial \sigma_I \partial \sigma_J \partial \sigma_K} \right)_0 \sigma_I(x) \sigma_J(x) \sigma_K(x) + \dots, \end{aligned} \quad (11)$$

where $(\partial^n \zeta / \partial \sigma_{I_1} \dots \partial \sigma_{I_n})_0$ are numbers representing the Taylor expansion of the generic relation, local in real space, between ζ and σ_I , $\zeta(\vec{x}) = f(\sigma_I(\vec{x}))$, around the point $\sigma_I = 0$. This relationship, developed in [4], generalizes in a non-trivial way the so-called δN formalism of [39–42].

At this point the problem of writing the effective field theory of multifield inflation is reduced to writing a Lagrangian for the additional light fields present during inflation, possibly coupled to the Goldstone boson π . Clearly, there is some freedom in what kind of fields we decide to include. In this paper we will content ourselves with the fields studied in [4], although it would be interesting to study additional possibilities. There, the additional fields that were included were scalar fields σ_I which generate curvature perturbations after horizon crossing, and not just through their effect on π .⁴ To ensure that quantum corrections are small and do not make the mass of these additional fields large, it was postulated that these fields were either the Goldstone bosons of some global symmetry, abelian or non-abelian, or they were protected by an approximate supersymmetry.⁵

These different mechanisms that protect the lightness of the additional scalar fields from quantum corrections can lead to distinguishable signals that, if detected, might allow us to infer the mechanism protecting the lightness of these fields, as described in detail in [4], to which we refer for details. Unfortunately, these mechanism-specific signals appear only as either subleading signals that have lower signal-to-noise ratio than other ones that should be detected first, or as signals appearing in correlation functions involving isocurvature fluctuations. Unfortunately, the leading signal is not able to distinguish among the various mechanisms protecting the lightness of the additional fields. Since in this paper we will restrict to adiabatic fluctuations, and since we are just trying to detect the leading signal, we can neglect all these distinctions, and we can focus on the following Lagrangian, which is common to all three mechanisms above (Abelian Goldstone bosons, non-Abelian Goldstone bosons, and supersymmetry):

$$S_\sigma = \int d^4x \sqrt{-g} \left[\frac{1}{2} (\partial_\mu \sigma)^2 + \frac{1}{\Lambda_1^4} \dot{\sigma}^4 + \frac{1}{\Lambda_2^4} \dot{\sigma}^2 (\partial_i \sigma)^2 + \frac{1}{\Lambda_3^4} (\partial_i \sigma)^2 (\partial_j \sigma)^2 + \frac{\mu^4}{\Lambda^4} \sigma^4 + \dots \right]. \quad (12)$$

This Lagrangian reproduces the relevant features that are contained in the models in [4]. First, notice that we did not write any cubic terms that would give rise to a bispectrum signature. These can be suppressed with some symmetry, such as for example a Z_2 symmetry $\sigma \rightarrow -\sigma$ or by imposing a Lorentz invariance in the theory, as described in [4]. The quartic couplings are suppressed by scales $\Lambda_{1,2,3}$, the smallest of which represents the unitarity bound of the theory. The first three interactions are compatible with a shift symmetry of the σ field, and their coefficients are all independent. This means that they can generate observable templates associated to the operators $\dot{\sigma}^4$, $\dot{\sigma}^2 (\partial_i \sigma)^2$ and

⁴ This means that our discussion does not include models of the class of the so-called quasi-single field inflation [43, 44]

⁵ Supersymmetry is broken during inflation minimally only by the Hubble scale H , which means that radiative corrections to the superpotential vanish above the scale. For weakly coupled theories, where loops are suppressed by a weak coupling parameter, this makes radiative corrections perturbatively small [4].

$(\partial_i\sigma)^2(\partial_j\sigma)^2$. Note that the operator $\dot{\sigma}^4$ generates the same trispectrum as the operator $\dot{\pi}^4$ considered previously in the single field case. The operator σ^4 is present in the case the σ fields are supersymmetric, or when the symmetry that the Goldstone bosons σ 's non-linearly realize is softly broken. This operator gives rise to a bispectrum of the local form which, again, cannot be generated in the single field case. The signal produced by the σ^4 term in the Lagrangian can give rise to a much larger signal than the one associated to an f_{NL}^{loc} of order unity. On top of these contributions, there are the ones associated to the non-linear relation between ζ and σ 's in Eq. (11). They give rise to bispectra and trispectra of local type.

Finally, we notice that one can enforce a particular symmetry in the case of multifield inflation, where non-Gaussianities are generated in a theory where Lorentz invariance in the multifield sector is left unbroken [4]. In this case, only two operators survive, $(\partial_\mu\sigma)^2(\partial_\nu\sigma)^2$ and σ^4 . This symmetry can be explicitly checked to be mapped into a conformal symmetry of the three-dimensional templates [45, 46]. There are finally additional trispectra, as for example $\sigma^2(\partial\sigma)^2$, associated to soft breaking of the some internal symmetries or to supersymmetry [4] whose analysis we defer to a subsequent work. Additional interesting studies, including some very early ones, for the inflationary trispectrum, both in single field and multifield inflation, can be found in [47–77].

We conclude this section by relating parameters in the above Lagrangians to the g_{NL} coefficients defined in the introduction. For the case of the single field Lagrangian (Eq. (9)), a short calculation using the in-in formalism [12] shows:

$$g_{NL}^{\dot{\sigma}^4} = \frac{25}{288} \frac{M_4^4}{H^4} A_\zeta c_s^3. \quad (13)$$

For the multifield Lagrangian (Eq. (12)), we find:

$$g_{NL}^{\dot{\sigma}^4} A_\zeta = \frac{25}{768} \frac{H^4}{\Lambda_1^4}, \quad g_{NL}^{\dot{\sigma}^2(\partial\sigma)^2} A_\zeta = -\frac{325}{6912} \frac{H^4}{\Lambda_2^4}, \quad g_{NL}^{(\partial\sigma)^4} A_\zeta = \frac{2575}{20736} \frac{H^4}{\Lambda_3^4}. \quad (14)$$

Notice that, as expected, $(g_{NL}^{\dot{\sigma}^4} A_\zeta)$, $(g_{NL}^{\dot{\sigma}^2(\partial\sigma)^2} A_\zeta)$, and $(g_{NL}^{(\partial\sigma)^4} A_\zeta)$ scale as $(H/\Lambda)^4$, being generated by dimension eight operators. The Lorentz invariant trispectrum generated by the operator $(\partial_\mu\sigma)^2(\partial_\nu\sigma)^2$ is obtained by setting $\Lambda_1^4 = \Lambda_3^4 = -2\Lambda_2^4$.

Finally, for the local trispectrum, we get either:

$$g_{NL}^{\text{loc}} A_\zeta = -\frac{50}{27} \frac{\mu^4}{\Lambda^4} N_e \left(1 + \mathcal{O}\left(\frac{1}{N_e}\right) \right) \quad (15)$$

in the case where the trispectrum is generated by a σ^4 interaction in the multifield action (Eq. (12)), or

$$g_{NL}^{\text{loc}} = \frac{25}{54} \frac{H^6}{A_\zeta^3} \left(\frac{\partial^3 \zeta}{\partial \sigma_I \partial \sigma_J \partial \sigma_K} \right)_0 \left(\frac{\partial \zeta}{\partial \sigma_I} \right)_0 \left(\frac{\partial \zeta}{\partial \sigma_J} \right)_0 \left(\frac{\partial \zeta}{\partial \sigma_K} \right)_0 \quad (16)$$

in the case where the local trispectrum is generated by the conversion mechanism in Eq. (11).

III. THE CMB TRISPECTRUM AND ITS OPTIMAL ESTIMATOR

A. Toy model

Before diving into the complications of the CMB, it may be illuminating to construct the optimal trispectrum estimator for the following toy model. Let x_1, \dots, x_N be independent identically distributed random variables whose distribution is nearly Gaussian, with mean zero, known variance σ^2 , and small kurtosis $\kappa \ll \sigma^4$ which we would like to estimate. Thus the two-point and four-point functions are:

$$\langle x_i x_j \rangle = \sigma^2 \delta_{ij} \quad \langle x_i x_j x_k x_l \rangle = \sigma^4 (\delta_{ij} \delta_{kl} + \delta_{ik} \delta_{jl} + \delta_{il} \delta_{jk}) + \kappa \delta_{ij} \delta_{jk} \delta_{kl} \quad (17)$$

It may seem natural to estimate κ using the simple estimator:

$$\hat{\kappa}_{\text{naive}} = \frac{1}{N} \left(\sum_{i=1}^N x_i^4 \right) - 3\sigma^4 \quad (18)$$

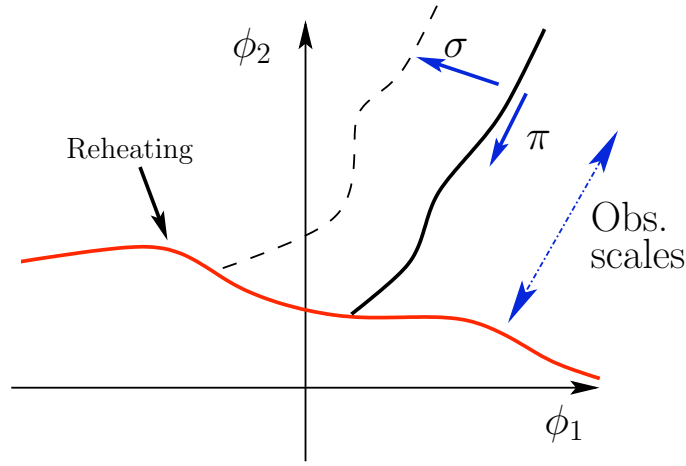


FIG. 1: Representation of a typical multifield potential. Modes of interest for observation cross the horizon about sixty e -foldings before the end of inflation. Therefore, effects coming from the evolution of the fields after horizon crossing can be treated locally in real space. The effective theory is more general than this example, as it does not assume that the inflaton is a scalar field. This example is however interesting in helping in visualizing the different scales in the problem.

However, this estimator is suboptimal! The optimal (minimum variance) estimator turns out to be

$$\hat{\kappa}_{\text{opt}} = \frac{1}{N} \left(\sum_{i=1}^N x_i^4 \right) - 6\sigma^2 \frac{1}{N} \left(\sum_{i=1}^N x_i^2 \right) + 3\sigma^4 \quad (19)$$

A short calculation using Wick's theorem shows that

$$\text{Var}(\hat{\kappa}_{\text{naive}}) = \frac{96\sigma^8}{N} \quad \text{Var}(\hat{\kappa}_{\text{opt}}) = \frac{24\sigma^8}{N} \quad (20)$$

so the naive estimator $\hat{\kappa}_{\text{naive}}$ is significantly suboptimal.

In addition to having lower variance, the optimal estimator has another property which is crucial in practice. Suppose that the variance σ^2 is not precisely known in advance, but has been estimated with some error $\Delta\sigma^2 = \sigma_{\text{est}}^2 - \sigma_{\text{true}}^2$. Let us compute the ‘‘two-point bias’’ in our estimate of κ due to the incorrectly estimated variance. A short calculation gives:

$$\langle \hat{\kappa}_{\text{naive}} \rangle = \kappa - 6\sigma^2(\Delta\sigma^2) + \mathcal{O}(\Delta\sigma^2)^2 \quad \langle \hat{\kappa}_{\text{opt}} \rangle = \kappa + 3(\Delta\sigma^2)^2 \quad (21)$$

In other words, the optimal estimator is *parametrically more robust* (by one power of $\Delta\sigma^2$) to errors in our estimates of the two-point function. This extra robustness will be important when we generalize to the CMB, where beams, noise, and residual foregrounds all contribute to the two-point function and are notoriously difficult to estimate precisely.

B. CMB estimator

Let us first establish some notation. We denote the angular four-point function or trispectrum of the CMB by:

$$\begin{aligned} T_{m_1 m_2 m_3 m_4}^{\ell_1 \ell_2 \ell_3 \ell_4} &= \langle a_{\ell_1 m_1} a_{\ell_2 m_2} a_{\ell_3 m_3} a_{\ell_4 m_4} \rangle_c \\ &= \langle a_{\ell_1 m_1} a_{\ell_2 m_2} a_{\ell_3 m_3} a_{\ell_4 m_4} \rangle - \langle a_{\ell_1 m_1} a_{\ell_2 m_2} \rangle \langle a_{\ell_3 m_3} a_{\ell_4 m_4} \rangle \\ &\quad - \langle a_{\ell_1 m_1} a_{\ell_3 m_3} \rangle \langle a_{\ell_2 m_2} a_{\ell_4 m_4} \rangle - \langle a_{\ell_1 m_1} a_{\ell_4 m_4} \rangle \langle a_{\ell_2 m_2} a_{\ell_3 m_3} \rangle \\ &= \langle a_{\ell_1 m_1} a_{\ell_2 m_2} a_{\ell_3 m_3} a_{\ell_4 m_4} \rangle - \left[(-1)^{m_1+m_3} C_{\ell_1} C_{\ell_3} \delta_{\ell_1 \ell_2} \delta_{\ell_3 \ell_4} \delta_{m_1, -m_3} \delta_{m_2, -m_4} + (2 \text{ perm.}) \right] \end{aligned} \quad (22)$$

The trispectrum $T_{m_1 m_2 m_3 m_4}^{\ell_1 \ell_2 \ell_3 \ell_4}$ is invariant under the 4! permutations of its indices (ℓ_i, m_i) , and satisfies the reality condition

$$T_{m_1 m_2 m_3 m_4}^{\ell_1 \ell_2 \ell_3 \ell_4*} = (-1)^{m_1+m_2+m_3+m_4} T_{(-m_1)(-m_2)(-m_3)(-m_4)}^{\ell_1 \ell_2 \ell_3 \ell_4} \quad (23)$$

We will only consider CMB trispectra which are rotationally invariant, i.e. $T_{m_1 m_2 m_3 m_4}^{\ell_1 \ell_2 \ell_3 \ell_4}$ is unchanged if a common rotation is applied to all four pairs of indices (ℓ_i, m_i) . This means that the trispectrum has fewer degrees of freedom than the index notation $T_{m_1 m_2 m_3 m_4}^{\ell_1 \ell_2 \ell_3 \ell_4}$ would suggest. (It is possible to devise alternate notation which makes this more explicit [78], but we will not do so in this paper.)

Now consider a CMB experiment in which the instrumental response is linear and the noise is Gaussian. The observed CMB $a_{\ell m}$ is a sum of signal and noise contributions: we have $a_{\ell m} = s_{\ell m} + n_{\ell m}$, where $s_{\ell m}$ is the true CMB and $n_{\ell m}$ is Gaussian noise. Let $C_{\ell_1 m_1, \ell_2 m_2} = \langle a_{\ell_1 m_1} a_{\ell_2 m_2} \rangle$ be the total (signal + noise) covariance of the observed CMB. Note that although the signal contribution to C will be diagonal in (ℓ, m) , the noise contribution will generally be nondiagonal.

Armed with the above notation, the optimal trispectrum estimator can be written in the following general form [79]:

$$\hat{\mathcal{E}} = \frac{1}{24F} \sum_{\ell_i m_i} T_{m_1 m_2 m_3 m_4}^{\ell_1 \ell_2 \ell_3 \ell_4 *} \left[(C^{-1}a)_{\ell_1 m_1} (C^{-1}a)_{\ell_2 m_2} (C^{-1}a)_{\ell_3 m_3} (C^{-1}a)_{\ell_4 m_4} \right. \\ \left. - 6 C_{\ell_1 m_1, \ell_2 m_2}^{-1} (C^{-1}a)_{\ell_3 m_3} (C^{-1}a)_{\ell_4 m_4} \right. \\ \left. + 3 C_{\ell_1 m_1, \ell_2 m_2}^{-1} C_{\ell_3 m_3, \ell_4 m_4}^{-1} \right] \quad (24)$$

where the normalizing constant F is given by

$$F = \frac{1}{4!} \sum_{\ell_i m_i \ell'_i m'_i} T_{m_1 m_2 m_3 m_4}^{\ell_1 \ell_2 \ell_3 \ell_4 *} C_{\ell_1 m_1, \ell'_1 m'_1}^{-1} C_{\ell_2 m_2, \ell'_2 m'_2}^{-1} C_{\ell_3 m_3, \ell'_3 m'_3}^{-1} C_{\ell_4 m_4, \ell'_4 m'_4}^{-1} T_{m'_1 m'_2 m'_3 m'_4}^{\ell'_1 \ell'_2 \ell'_3 \ell'_4} \quad (25)$$

Let us now interpret the terms in the optimal estimator above. The first (quartic) term on the RHS of Eq. (24) is a sum over 4-tuples (ℓ_i, m_i) in which each 4-tuple is weighted by the template signal $T_{m_1 m_2 m_3 m_4}^{\ell_1 \ell_2 \ell_3 \ell_4}$, and inversely weighted by the total covariance C . This type of weighting appears in a variety of optimal CMB estimators, for example optimal estimators for the power spectrum or bispectrum. The second (quadratic) and third (constant) terms in Eq. (24) parallel the terms found previously for the toy model in Eq. (19). We note that a similar structure occurs in the optimal estimator for the three-point function, where there is a one-point term in addition to the leading three-point term [5].

As in the toy model, the additional terms in Eq. (24) reduce the variance, and also make the estimator more robust to errors in the two-point function. To make this last point more precise, if the total covariance C is estimated incorrectly with nonzero error ΔC , then it is easy to show that the bias in the estimator is parametrically $\mathcal{O}((\Delta C)^2)$ rather than $\mathcal{O}(\Delta C)$. This property is critical in practice. If we used an estimator whose bias is parametrically $\mathcal{O}(\Delta C)$, we would need to model beams, noise bias, residual foregrounds, etc. with fractional accuracy $1/\ell_{\max} \approx 0.1\%$. This level of accuracy is extremely difficult to achieve for an experiment as complex as Planck. On the other hand, with an estimator whose bias is parametrically $\mathcal{O}(\Delta C^2)$, the required fractional accuracy is $\approx 1/\ell_{\max}^{1/2}$ or a few percent, which is easily achieved in practice.

A short calculation shows that the variance of the optimal estimator is

$$\text{Var}(\hat{\mathcal{E}}) = \frac{1}{F} \quad (26)$$

i.e. F determines both the normalization of the estimator and its variance.

C. The Q -symbol

We now define notation which will be used ubiquitously throughout the paper. Given a CMB trispectrum $T_{m_1 m_2 m_3 m_4}^{\ell_1 \ell_2 \ell_3 \ell_4}$ and CMB realization $a_{\ell m}$, we define the “ Q -symbol” $Q_T[a]$ by:

$$Q_T[a] = \frac{1}{4!} \sum_{\ell_i m_i} T_{m_1 m_2 m_3 m_4}^{\ell_1 \ell_2 \ell_3 \ell_4 *} a_{\ell_1 m_1} a_{\ell_2 m_2} a_{\ell_3 m_3} a_{\ell_4 m_4} \quad (27)$$

The reality condition (23) for the trispectrum, together with the reality condition $a_{\ell m}^* = (-1)^m a_{\ell(-m)}$, implies that $Q_T[a]$ is real. Note that a similar notation $T[a]$ was defined for the bispectrum in [21].

This notation is useful since most of the machinery in this paper can be written purely in terms of the Q -symbol. Therefore, our machinery applies to a trispectrum if a fast algorithm exists for evaluating its Q -symbol. For example, the optimal estimator from the previous section can be written as the following Monte Carlo average:

$$\widehat{\mathcal{E}}[a] = \frac{1}{F} \left(Q[C^{-1}a, C^{-1}a, C^{-1}a, C^{-1}a] - 6 \left\langle Q[C^{-1}a, C^{-1}a, C^{-1}b, C^{-1}b] \right\rangle_b + \left\langle Q[C^{-1}b, C^{-1}b, C^{-1}b, C^{-1}b] \right\rangle_b \right) \quad (28)$$

where $\langle \cdot \rangle_b$ denotes an average over Gaussian random realizations b with covariance matrix C . In §VI we will develop fast algorithms for computing Fisher matrices, and in §IX we will present detailed data analysis pipelines, under the assumption that $Q_T[a]$ is computable. We will also present an algorithm for simulating a non-Gaussian map with specified trispectrum, although we defer this to Appendix B since it is somewhat peripheral to our goal of analyzing WMAP data.

We define the gradient $\partial_{\ell m} Q_T[a]$ by:

$$\partial_{\ell m} Q_T[a] = \frac{\partial Q_T[a]}{\partial a_{\ell m}^*} = \frac{1}{3!} \sum_{\ell_i m_i} T_{m m_1 m_2 m_3}^{\ell \ell_1 \ell_2 \ell_3} a_{\ell_1 m_1}^* a_{\ell_2 m_2}^* a_{\ell_3 m_3}^* \quad (29)$$

The object $\partial_{\ell m} Q_T[a]$ is a harmonic-space map, as the index notation suggests. It transforms covariantly under rotations, in the sense that $\partial Q[R \cdot a] = R \cdot \partial Q[a]$, where $(R \cdot a)$ denotes the action of a rotation $R \in SO(3)$ on a harmonic-space map $a_{\ell m}$.

We will sometimes omit the subscript T , and simply write $Q[a]$ or $\partial_{\ell m} Q[a]$, if the trispectrum is understood. It will also be convenient to define the following generalizations of Q and ∂Q , which are functions of four CMB realizations (a, b, c, d) and three realizations (a, b, c) respectively:

$$\begin{aligned} Q_T[a, b, c, d] &= \frac{1}{4!} \sum_{\ell_i m_i} T_{m_1 m_2 m_3 m_4}^{\ell_1 \ell_2 \ell_3 \ell_4} a_{\ell_1 m_1} b_{\ell_2 m_2} c_{\ell_3 m_3} d_{\ell_4 m_4} \\ \partial_{\ell m} Q_T[a, b, c] &= \frac{1}{3!} \sum_{\ell_i m_i} T_{m m_1 m_2 m_3}^{\ell \ell_1 \ell_2 \ell_3} a_{\ell_1 m_1}^* b_{\ell_2 m_2}^* c_{\ell_3 m_3}^* \end{aligned} \quad (30)$$

D. An alternate approach?

Let us temporarily return to the toy model from III A. We construct an interesting near-optimal trispectrum estimator as follows. Suppose we use the naive estimator $\widehat{\kappa}_{\text{naive}}$, but estimate the variance σ^2 internally from data, rather than assuming a priori knowledge of σ^2 . In other words, consider the pure four-point estimator:

$$\widehat{\kappa}_{\text{alt}} = \frac{1}{N} \left(\sum_i x_i^4 \right) - \frac{3}{N(N-1)} \left(\sum_{i \neq j} x_i^2 x_j^2 \right) \quad (31)$$

It is not hard to show that the variance is

$$\text{Var}(\widehat{\kappa}_{\text{alt}}) = \frac{24\sigma^8}{N} \left(1 + \frac{3}{N-1} \right) \quad (32)$$

Comparing with the result for the optimal estimator (Eq. (19)) we see that $\widehat{\kappa}_{\text{alt}}$ is near-optimal, in the sense that its variance agrees with the optimal estimator to leading order in $1/N$. This estimator also has the property that its two-point bias (due to incorrectly estimated σ^2) is zero! The estimator $\widehat{\kappa}_{\text{alt}}$ is only sensitive to the four-point signal κ , with no dependence on the variance σ^2 . We note that this statement does assume that the covariance matrix of the x_i is proportional to the identity matrix, and there is no estimator which has zero bias for an arbitrary covariance matrix C_{ij} . Nevertheless it is interesting that a zero-bias estimator exists for a restricted form of covariance matrix, and natural to ask whether this generalizes to the CMB context.

Ideally we would like to construct a CMB trispectrum estimator which is unbiased if either (1) the isotropic signal power spectrum C_ℓ , or (2) the noise covariance is estimated incorrectly. We speculate that it is possible to give a general construction of such an estimator. Noise bias can be eliminated by dividing the data into subsets with uncorrelated noise, making maps $(a_1)_{\ell m}, (a_2)_{\ell m}, \dots$ from one subset at a time, and allowing only “cross” terms $Q[a_i, a_j, a_k, a_l]$ with (i, j, k, l) distinct. Signal bias can be eliminated by estimating C_ℓ directly from the data and subtracting a term which is quadratic in the *estimated* C_ℓ ’s, by analogy with the toy model case above. Such an estimator would be very useful e.g. for the gravitational lensing four-point function, where a variety of noise bias cancelling schemes have been proposed [25, 80–82]. However, we defer this topic for future work.

IV. 3D → 2D PROJECTION

We will often be interested in “primordial” trispectra, that is, CMB trispectra which arise by linearly evolving a physically motivated four-point function in the 3D adiabatic initial curvature ζ . The ζ -trispectrum is defined by:

$$\begin{aligned} \langle \zeta_{\mathbf{k}_1} \zeta_{\mathbf{k}_2} \zeta_{\mathbf{k}_3} \zeta_{\mathbf{k}_4} \rangle_c &= \langle \zeta_{\mathbf{k}_1} \zeta_{\mathbf{k}_2} \zeta_{\mathbf{k}_3} \zeta_{\mathbf{k}_4} \rangle - \langle \zeta_{\mathbf{k}_1} \zeta_{\mathbf{k}_2} \rangle \langle \zeta_{\mathbf{k}_3} \zeta_{\mathbf{k}_4} \rangle - \langle \zeta_{\mathbf{k}_1} \zeta_{\mathbf{k}_3} \rangle \langle \zeta_{\mathbf{k}_2} \zeta_{\mathbf{k}_4} \rangle - \langle \zeta_{\mathbf{k}_1} \zeta_{\mathbf{k}_4} \rangle \langle \zeta_{\mathbf{k}_2} \zeta_{\mathbf{k}_3} \rangle \\ &= \langle \zeta_{\mathbf{k}_1} \zeta_{\mathbf{k}_2} \zeta_{\mathbf{k}_3} \zeta_{\mathbf{k}_4} \rangle - \left[P(k_1)P(k_3)(2\pi)^6 \delta^3(\mathbf{k}_1 + \mathbf{k}_2) \delta^3(\mathbf{k}_3 + \mathbf{k}_4) + (2 \text{ perm.}) \right] \end{aligned} \quad (33)$$

We will also use the “primed” notation $\langle \zeta_{\mathbf{k}_1} \zeta_{\mathbf{k}_2} \zeta_{\mathbf{k}_3} \zeta_{\mathbf{k}_4} \rangle'$ to denote the ζ -trispectrum without its momentum-conserving delta function, i.e.

$$\langle \zeta_{\mathbf{k}_1} \zeta_{\mathbf{k}_2} \zeta_{\mathbf{k}_3} \zeta_{\mathbf{k}_4} \rangle_c = \langle \zeta_{\mathbf{k}_1} \zeta_{\mathbf{k}_2} \zeta_{\mathbf{k}_3} \zeta_{\mathbf{k}_4} \rangle' (2\pi)^3 \delta^3\left(\sum \mathbf{k}_i\right) \quad (34)$$

We can project a ζ -trispectrum to an angular CMB trispectrum as follows. Recall that the CMB multipoles $a_{\ell m}$ are related to the initial curvature ζ by:

$$a_{\ell m} = 4\pi i^\ell \int \frac{d^3 \mathbf{k}}{(2\pi)^3} \Delta_\ell(k) \zeta(\mathbf{k}) Y_{\ell m}^*(\hat{\mathbf{k}}) \quad (35)$$

where the transfer function $\Delta_\ell(k)$ defined by this equation can be computed numerically using CAMB [83]. The following general trispectrum projection formula follows immediately:

$$T_{m_1 m_2 m_3 m_4}^{\ell_1 \ell_2 \ell_3 \ell_4} = \int \frac{d^3 \mathbf{k}_1 d^3 \mathbf{k}_2 d^3 \mathbf{k}_3 d^3 \mathbf{k}_4}{(2\pi)^{12}} \langle \zeta_{\mathbf{k}_1} \zeta_{\mathbf{k}_2} \zeta_{\mathbf{k}_3} \zeta_{\mathbf{k}_4} \rangle_c \prod_{i=1}^4 \left(4\pi i^{\ell_i} \Delta_{\ell_i}(k_i) Y_{\ell_i m_i}^*(\hat{\mathbf{k}}_i) \right) \quad (36)$$

Plugging this into the definition (27) of the Q -symbol, we get the following expression for $Q_T[a]$:

$$Q_T[a] = \frac{1}{4!} \int \frac{d^3 \mathbf{k}_1 d^3 \mathbf{k}_2 d^3 \mathbf{k}_3 d^3 \mathbf{k}_4}{(2\pi)^{12}} \langle \zeta_{\mathbf{k}_1} \zeta_{\mathbf{k}_2} \zeta_{\mathbf{k}_3} \zeta_{\mathbf{k}_4} \rangle_c^* \prod_{i=1}^4 \left(\sum_{\ell_i m_i} 4\pi (-i)^{\ell_i} \Delta_{\ell_i}(k_i) a_{\ell_i m_i} Y_{\ell_i m_i}(\hat{\mathbf{k}}_i) \right) \quad (37)$$

Since the functional form of $Q_T[a]$ uniquely determines $T_{m_1 m_2 m_3 m_4}^{\ell_1 \ell_2 \ell_3 \ell_4}$, this expression for Q_T is equivalent to the projection formula (36) for T . In fact, throughout the paper we will often find it more convenient to specify a trispectrum T by giving a formula for $Q_T[a]$ than by an explicit expression for $T_{m_1 m_2 m_3 m_4}^{\ell_1 \ell_2 \ell_3 \ell_4}$.

V. FACTORIZABILITY

Evaluating $Q_T[a]$ directly from its harmonic-space definition (27) is computationally intractable, since the number of terms in the sum is $\mathcal{O}(\ell_{\max}^7)$, where $\ell_{\max} = \mathcal{O}(10^3)$ for WMAP or Planck. An analogous computational problem arises in analysis of the CMB bispectrum, where it has been solved using the idea of finding a *factorizable representation* of the bispectrum. We start by briefly reviewing factorizability for the bispectrum, in notation which will set the stage for the trispectrum discussion to follow.

A. Review of factorizability for the bispectrum

A CMB three-point function is said to be *factorizable* if it is a sum of terms of the form:

$$\langle a_{\ell_1 m_1} a_{\ell_2 m_2} a_{\ell_3 m_3} \rangle = \sum_{I=1}^{N_{\text{fact}}} A_{\ell_1}^I B_{\ell_2}^I C_{\ell_3}^I \mathcal{G}_{m_1 m_2 m_3}^{\ell_1 \ell_2 \ell_3} + (5 \text{ perm.}) \quad (38)$$

where $A_\ell^I, B_\ell^I, C_\ell^I$ are N_{fact} -by- ℓ_{\max} real-valued matrices, and $\mathcal{G}_{m_1 m_2 m_3}^{\ell_1 \ell_2 \ell_3}$ is the Gaunt symbol, defined by:

$$\begin{aligned} \mathcal{G}_{m_1 m_2 m_3}^{\ell_1 \ell_2 \ell_3} &= \int d^2 \hat{\mathbf{n}} Y_{\ell_1 m_1}(\hat{\mathbf{n}}) Y_{\ell_2 m_2}(\hat{\mathbf{n}}) Y_{\ell_3 m_3}(\hat{\mathbf{n}}) \\ &= \sqrt{\frac{(2\ell_1 + 1)(2\ell_2 + 1)(2\ell_3 + 1)}{4\pi}} \begin{pmatrix} \ell_1 & \ell_2 & \ell_3 \\ 0 & 0 & 0 \end{pmatrix} \end{aligned} \quad (39)$$

The significance of the factorizability condition is that it makes the bispectrum estimator computationally feasible. First recall [21] that the bispectrum estimator can be written in terms of the T -symbol, defined by:

$$T[a] = \frac{1}{6} \sum_{\ell_i m_i} \langle a_{\ell_1 m_1} a_{\ell_2 m_2} a_{\ell_3 m_3} \rangle^* a_{\ell_1 m_1} a_{\ell_2 m_2} a_{\ell_3 m_3} \quad (40)$$

This harmonic-space sum is computationally infeasible, but if the bispectrum satisfies the factorizability condition (38) then $T[a]$ can be rewritten:

$$T[a] = \sum_{I=1}^{N_{\text{fact}}} \int d^2 \hat{\mathbf{n}} \left(\sum_{\ell_1 m_1} A_{\ell_1}^I a_{\ell_1 m_1} Y_{\ell_1 m_1}(\hat{\mathbf{n}}) \right) \left(\sum_{\ell_2 m_2} B_{\ell_2}^I a_{\ell_2 m_2} Y_{\ell_2 m_2}(\hat{\mathbf{n}}) \right) \left(\sum_{\ell_3 m_3} C_{\ell_3}^I a_{\ell_3 m_3} Y_{\ell_3 m_3}(\hat{\mathbf{n}}) \right) \quad (41)$$

which is straightforward to evaluate efficiently using fast spherical transforms. For this reason, finding a factorizable representation for a given bispectrum is the key to making data analysis practically feasible.

Many CMB bispectra of interest arise from 3D \rightarrow 2D projection of a ζ -bispectrum $\langle \zeta_{\mathbf{k}_1} \zeta_{\mathbf{k}_2} \zeta_{\mathbf{k}_3} \rangle$. There is also a useful notion of factorizability for a ζ -bispectrum as follows. A ζ -bispectrum $\langle \zeta_{\mathbf{k}_1} \zeta_{\mathbf{k}_2} \zeta_{\mathbf{k}_3} \rangle$ is said to be factorizable if:

$$\langle \zeta_{\mathbf{k}_1} \zeta_{\mathbf{k}_2} \zeta_{\mathbf{k}_3} \rangle' = \frac{1}{6} \sum_{I=1}^{N_{\text{fact}}} \alpha_I(k_1) \beta_I(k_2) \gamma_I(k_3) + (5 \text{ perm.}) \quad (42)$$

where $\alpha_I(k), \beta_I(k), \gamma(k)$ are arbitrary functions. A general 3D \rightarrow 2D projection formula for bispectra, very similar to the one given for trispectra in the last section, shows that the corresponding CMB bispectrum is:

$$\begin{aligned} \langle a_{\ell_1 m_1} a_{\ell_2 m_2} a_{\ell_3 m_3} \rangle &= \frac{1}{6} \sum_{I=1}^{N_{\text{fact}}} \int r^2 dr \left(\int \frac{2k_1^2 dk_1}{\pi} j_{\ell_1}(k_1 r) \Delta_{\ell_1}(k_1) \alpha_I(k_1) \right) \\ &\quad \times \left(\int \frac{2k_2^2 dk_2}{\pi} j_{\ell_2}(k_2 r) \Delta_{\ell_2}(k_2) \beta_I(k_2) \right) \\ &\quad \times \left(\int \frac{2k_3^2 dk_3}{\pi} j_{\ell_3}(k_3 r) \Delta_{\ell_3}(k_3) \gamma_I(k_3) \right) \mathcal{G}_{m_1 m_2 m_3}^{\ell_1 \ell_2 \ell_3} + (5 \text{ perm.}) \end{aligned} \quad (43)$$

This equation shows that if we approximate the r integral by a finite sum, we obtain a CMB bispectrum which is factorizable in the sense defined by Eq. (38). Thus a ζ -bispectrum which is factorizable gives rise to a CMB bispectrum which is also factorizable, although the number of terms will increase by a large factor, since many points will be needed to approximate the r -integral.

A variety of general schemes have been proposed in the literature for making bispectrum data analysis computationally feasible (e.g. [8, 21–24]). These schemes can all be viewed as different proposals for representing a bispectrum as a sum of factorizable terms. Some methods operate directly on the CMB bispectrum, for example the binned estimator in [22] uses bandpowers in ℓ to define basis functions $A_{\ell}^I, B_{\ell}^I, C_{\ell}^I$. Other methods operate on the ζ -bispectrum before 3D \rightarrow 2D projection, for example by expanding the ζ -bispectrum in a set of orthogonal basis functions [8, 24]. Finally, in some cases it is possible to find an approximate factorizable representation as a pure ansatz. The canonical example is the equilateral bispectrum [5], where the factorizable template:

$$\langle \zeta_{\mathbf{k}_1} \zeta_{\mathbf{k}_2} \zeta_{\mathbf{k}_3} \rangle' = \frac{(k_1 + k_2 - k_3)(k_2 + k_3 - k_1)(k_3 + k_1 - k_2)}{k_1^3 k_2^3 k_3^3} \quad (44)$$

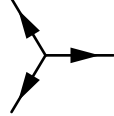
is 99% correlated to the exact bispectrum of the operator $\hat{\pi}^3$.

In this paper, we will concentrate on a “physical” approach to factorizability which generalizes nicely to the trispectrum and also provides some physical interpretation. The idea is that the Feynman diagram which one evaluates to compute a given bispectrum automatically supplies a factorizable representation. To illustrate this idea by example, consider the $\hat{\pi}^3$ bispectrum:

$$\langle \zeta_{\mathbf{k}_1} \zeta_{\mathbf{k}_2} \zeta_{\mathbf{k}_3} \rangle' \propto \frac{1}{k_1 k_2 k_3 (k_1 + k_2 + k_3)^3} \quad (45)$$

This bispectrum does not appear to be factorizable. However, let us go back to the Feynman diagram which produced

it:



$$\propto \int_{-\infty}^0 d\tau_E \tau_E^2 \left(\frac{e^{k_1 \tau_E}}{k_1} \right) \left(\frac{e^{k_2 \tau_E}}{k_2} \right) \left(\frac{e^{k_3 \tau_E}}{k_3} \right) \quad (46)$$


$$= \frac{2}{k_1 k_2 k_3 (k_1 + k_2 + k_3)^3} \quad (47)$$

Here, τ_E is Wick-rotated conformal time, which we take throughout this paper to run from $\tau_E = -\infty$ to 0. We see that the integrand in Eq. (46) is factorizable in k_1, k_2, k_3 . This is not a coincidence: it arises from combinatorics of the Feynman diagram, since each factor corresponds to one external line. If we do not evaluate the τ_E integral, but instead approximate it by a finite sum of τ_E values, then we will obtain a factorizable ζ -bispectrum. As shown in [21], the number of terms in the sum can be kept manageable by sampling the integral with equal spacing in $\log |\tau_E|$. This trick is general and shows that any CMB bispectrum which arises from a cubic diagram of the combinatorial type shown in Eq. (46) is factorizable, although the number of terms in the CMB bispectrum may be large, since we get one term for every sampling point needed to do the (τ_E, r) double integral.

B. Factorizability for the trispectrum

We would like to define a notion of factorizability for the *trispectrum*, in order to make data analysis of primordial trispectra computationally feasible.

We have just seen that in the bispectrum case, the notion of factorizability derives from the combinatorics of the Feynman diagram. In the trispectrum case, the trispectrum can come from either a “contact” diagram with a quartic vertex, or an “exchange” diagram with two cubic vertices:



$$\quad (48)$$

Accordingly, we will define two different factorizability conditions for the trispectrum, “contact factorizability” and “exchange factorizability”. We will give the precise definitions shortly, but there is one feature which can be anticipated in advance. One might think (by analogy with the bispectrum case) that a contact diagram always gives rise to a trispectrum of the form

$$\langle \zeta_{\mathbf{k}_1} \zeta_{\mathbf{k}_2} \zeta_{\mathbf{k}_3} \zeta_{\mathbf{k}_4} \rangle' = \int_{-\infty}^0 d\tau_E \alpha(k_1) \beta(k_2) \gamma(k_3) \delta(k_4) \quad (49)$$

in which the integrand is a factorizable function of $k_i = |\mathbf{k}_i|$. However, this is not fully general: if the quartic operator contains spatial derivatives, then there will be additional factors $(\mathbf{k}_i \cdot \mathbf{k}_j)$, as can be seen by inspection of Eqs. (6), (7) in the introduction. In the bispectrum case, we would be able to get rid of a factor such as $(\mathbf{k}_1 \cdot \mathbf{k}_2)$ by using the momentum-conserving delta function $\delta^3(\mathbf{k}_1 + \mathbf{k}_2 + \mathbf{k}_3)$ to write $(\mathbf{k}_1 \cdot \mathbf{k}_2) = (k_3^2 - k_1^2 - k_2^2)/2$ and reduce to the case in which the integrand is factorizable in $k_i = |\mathbf{k}_i|$. In the trispectrum case, there is no analogous way to eliminate factors $(\mathbf{k}_i \cdot \mathbf{k}_j)$. The consequence is that our definition of factorizability will contain non-scalar quantities, i.e. 2D fields with spin $s > 0$. This is a significant complication compared to the bispectrum case. For reference, the mathematics of spin- s fields is briefly reviewed in Appendix A.

C. Contact factorizability

In this section we give the formal definition of contact factorizability. We define an angular trispectrum $T_{m_1 m_2 m_3 m_4}^{\ell_1 \ell_2 \ell_3 \ell_4}$ to be “contact factorizable” if:

$$\begin{aligned} T_{m_1 m_2 m_3 m_4}^{\ell_1 \ell_2 \ell_3 \ell_4} &= \frac{1}{48} \sum_{I=1}^{N_{\text{fact}}} A_{\ell_1}^I B_{\ell_2}^I C_{\ell_3}^I D_{\ell_4}^I \int d^2 \hat{\mathbf{n}} (\alpha_I Y_{\ell_1 m_1}(\hat{\mathbf{n}})) (\beta_I Y_{\ell_2 m_2}(\hat{\mathbf{n}})) (\gamma_I Y_{\ell_3 m_3}(\hat{\mathbf{n}})) (\delta_I Y_{\ell_4 m_4}(\hat{\mathbf{n}})) \\ &+ (23 \text{ perm.}) + (\text{c.c.}) \end{aligned} \quad (50)$$

where $({}_s Y_{\ell m})$ denotes a spin- s spherical harmonic (Appendix A), $\alpha_I, \beta_I, \gamma_I, \delta_I$ are integer spins, and $A_\ell^I, B_\ell^I, C_\ell^I, D_\ell^I$ are N_{fact} -by- ℓ_{max} matrices. We will assume that $\alpha_I + \beta_I + \gamma_I + \delta_I = 0$ for each I so that the integrand in Eq. (50) has total spin zero.

Equivalently, we can define a contact factorizable trispectrum by the functional form of $Q_T[a]$.

$$Q_T[a] = \frac{1}{48} \sum_{I=1}^{N_{\text{fact}}} \int d^2 \hat{\mathbf{n}} \left(\sum_{\ell_1 m_1} A_{\ell_1}^I a_{\ell_1 m_1}(\alpha_I Y_{\ell_1 m_1}(\hat{\mathbf{n}})) \right) \left(\sum_{\ell_2 m_2} B_{\ell_2}^I a_{\ell_2 m_2}(\beta_I Y_{\ell_2 m_2}(\hat{\mathbf{n}})) \right) \\ \times \left(\sum_{\ell_3 m_3} C_{\ell_3}^I a_{\ell_3 m_3}(\gamma_I Y_{\ell_3 m_3}(\hat{\mathbf{n}})) \right) \left(\sum_{\ell_4 m_4} D_{\ell_4}^I a_{\ell_4 m_4}(\delta_I Y_{\ell_4 m_4}(\hat{\mathbf{n}})) \right) + \text{c.c.} \quad (51)$$

This definition of factorizability is useful because it is specific enough that there is a fast algorithm for evaluating $Q[a]$ (by straightforward use of Eq.(51) with fast spherical transforms), yet general enough that many physically interesting trispectra are contact factorizable.

We illustrate this by example, by showing that the operator $\hat{\sigma}^2(\partial\sigma)^2$ from the previous section is contact factorizable. We start from the ‘‘unintegrated’’ form of the trispectrum in the first line of Eq. (6):

$$\langle \zeta_{\mathbf{k}_1} \zeta_{\mathbf{k}_2} \zeta_{\mathbf{k}_3} \zeta_{\mathbf{k}_4} \rangle_c = -\frac{13824}{325} g_{NL}^{\hat{\sigma}^2(\partial\sigma)^2} A_\zeta^3 \int_{-\infty}^0 d\tau_E \tau_E^2 \frac{e^{\sum k_i \tau_E}}{k_1^3 k_2^3 k_3^3 k_4^3} (1 - k_1 \tau_E)(1 - k_2 \tau_E) (\mathbf{k}_1 \cdot \mathbf{k}_2) (2\pi)^3 \delta^3\left(\sum \mathbf{k}_i\right) + 5 \text{ perm.} \quad (52)$$

We plug this into the 3D \rightarrow 2D projection formula (37) to obtain an expression for $Q[a]$. We replace the momentum-conserving delta function $(2\pi)^3 \delta^3(\sum \mathbf{k}_i)$ by $\int d^3 \mathbf{r} \exp(i \sum \mathbf{k}_i \cdot \mathbf{r})$, and then replace the dot product $(\mathbf{k}_1 \cdot \mathbf{k}_2)$ by an appropriately placed pair of derivatives with respect to r . We obtain:

$$Q[a] = \frac{3456}{325} g_{NL}^{\hat{\sigma}^2(\partial\sigma)^2} A_\zeta^3 \int_{-\infty}^0 d\tau_E \tau_E^2 d^3 \mathbf{r} \left(\frac{\partial}{\partial \mathbf{r}_i} \sum_{\ell_1 m_1} \int \frac{d^3 \mathbf{k}_1}{(2\pi)^3} 4\pi(-i)^{\ell_1} \frac{(1 - k_1 \tau_E) e^{k_1 \tau_E}}{k_1^3} \Delta_{\ell_1}(k_1) e^{i \mathbf{k}_1 \cdot \mathbf{r}} a_{\ell_1 m_1} Y_{\ell_1 m_1}(\hat{\mathbf{k}}_1) \right) \\ \times \left(\frac{\partial}{\partial \mathbf{r}_i} \sum_{\ell_2 m_2} \int \frac{d^3 \mathbf{k}_2}{(2\pi)^3} 4\pi(-i)^{\ell_2} \frac{(1 - k_2 \tau_E) e^{k_2 \tau_E}}{k_2^3} \Delta_{\ell_2}(k_2) e^{i \mathbf{k}_2 \cdot \mathbf{r}} a_{\ell_2 m_2} Y_{\ell_2 m_2}(\hat{\mathbf{k}}_2) \right) \\ \times \left(\sum_{\ell_3 m_3} \int \frac{d^3 \mathbf{k}_3}{(2\pi)^3} 4\pi(-i)^{\ell_3} \frac{e^{k_3 \tau_E}}{k_3} \Delta_{\ell_3}(k_3) e^{i \mathbf{k}_3 \cdot \mathbf{r}} a_{\ell_3 m_3} Y_{\ell_3 m_3}(\hat{\mathbf{k}}_3) \right) \\ \times \left(\sum_{\ell_4 m_4} \int \frac{d^3 \mathbf{k}_4}{(2\pi)^3} 4\pi(-i)^{\ell_4} \frac{e^{k_4 \tau_E}}{k_4} \Delta_{\ell_4}(k_4) e^{i \mathbf{k}_4 \cdot \mathbf{r}} a_{\ell_4 m_4} Y_{\ell_4 m_4}(\hat{\mathbf{k}}_4) \right) \quad (53)$$

Following a standard trick [20], the next step is to Rayleigh expand each exponential as $\exp(i \mathbf{k}_i \cdot \mathbf{r}) = 4\pi \sum_{\ell m} i^\ell j_\ell(k_i r) Y_{\ell m}(\hat{\mathbf{r}}) Y_{\ell m}^*(\hat{\mathbf{k}})$ and do the angular parts of the k -integrals, obtaining:

$$Q[a] = \frac{3456}{325} g_{NL}^{\hat{\sigma}^2(\partial\sigma)^2} A_\zeta^3 \int_{-\infty}^0 d\tau_E \tau_E^2 d^3 \mathbf{r} \left(\frac{\partial}{\partial \mathbf{r}_i} \sum_{\ell_1 m_1} \int \frac{2k_1^2 dk_1}{\pi} \frac{(1 - k_1 \tau_E) e^{k_1 \tau_E}}{k_1^3} \Delta_{\ell_1}(k_1) j_{\ell_1}(k_1 r) a_{\ell_1 m_1} Y_{\ell_1 m_1}(\hat{\mathbf{r}}) \right) \\ \times \left(\frac{\partial}{\partial \mathbf{r}_i} \sum_{\ell_2 m_2} \int \frac{2k_2^2 dk_2}{\pi} \frac{(1 - k_2 \tau_E) e^{k_2 \tau_E}}{k_2^3} \Delta_{\ell_2}(k_2) j_{\ell_2}(k_2 r) a_{\ell_2 m_2} Y_{\ell_2 m_2}(\hat{\mathbf{r}}) \right) \\ \times \left(\sum_{\ell_3 m_3} \int \frac{2k_3^2 dk_3}{\pi} \frac{e^{k_3 \tau_E}}{k_3} \Delta_{\ell_3}(k_3) j_{\ell_3}(k_3 r) a_{\ell_3 m_3} Y_{\ell_3 m_3}(\hat{\mathbf{r}}) \right) \\ \times \left(\sum_{\ell_4 m_4} \int \frac{2k_4^2 dk_4}{\pi} \frac{e^{k_4 \tau_E}}{k_4} \Delta_{\ell_4}(k_4) j_{\ell_4}(k_4 r) a_{\ell_4 m_4} Y_{\ell_4 m_4}(\hat{\mathbf{r}}) \right) \quad (54)$$

Next we split the dot product of gradients $\sum_i \frac{\partial f}{\partial \mathbf{r}_i} \frac{\partial f}{\partial \mathbf{r}_i}$, as a sum of two terms: a term in which both derivatives act in the radial direction, and a term containing angular derivatives. More formally, we can write:

$$\sum_i \frac{\partial f(\mathbf{r})}{\partial \mathbf{r}_i} \frac{\partial f(\mathbf{r})}{\partial \mathbf{r}_i} = \left(\frac{\partial f(\mathbf{r})}{\partial r} \right)^2 + \frac{1}{r^2} (\hat{\sigma} f)^* (\hat{\sigma} f) \quad (55)$$

where $f(\mathbf{r})$ is any scalar-valued function and ∂ is the spin-raising operator (see Appendix A). Plugging this in we get:

$$Q[a] = \frac{384}{13} g_{NL}^{\dot{\sigma}^2(\partial\sigma)^2} \int_{-\infty}^0 d\tau_E \int_0^\infty dr \int d^2\hat{\mathbf{n}} \tau_E^2 r^2 \left(\sum_{\ell m} \mu_\ell(\tau_E, r) a_{\ell m} Y_{\ell m}(\hat{\mathbf{n}}) \right)^2 \times \left[\left(\sum_{\ell' m'} \nu_{\ell'}(\tau_E, r) a_{\ell' m'} Y_{\ell' m'}(\hat{\mathbf{n}}) \right)^2 + \left| \sum_{\ell' m'} \omega_{\ell'}(\tau_E, r) a_{\ell' m'} ({}_1Y_{\ell' m'}(\hat{\mathbf{n}})) \right|^2 \right] \quad (56)$$

where we have used the identity $\partial Y_{\ell m} = \sqrt{\ell(\ell+1)} ({}_1Y_{\ell m})$ and defined

$$\begin{aligned} \mu_\ell(\tau_E, r) &= \left(\frac{3}{5}\right)^{1/2} \int \frac{2k^2 dk}{\pi} e^{k\tau_E} k^{5/4} P_\zeta(k)^{3/4} \Delta_\ell(k) j_\ell(kr) \\ \nu_\ell(\tau_E, r) &= \left(\frac{3}{5}\right)^{1/2} \int \frac{2k^2 dk}{\pi} (1 - k\tau_E) e^{k\tau_E} k^{1/4} P_\zeta(k)^{3/4} \Delta_\ell(k) j'_\ell(kr) \\ \omega_\ell(\tau_E, r) &= \frac{\sqrt{\ell(\ell+1)}}{r} \left(\frac{3}{5}\right)^{1/2} \int \frac{2k^2 dk}{\pi} (1 - k\tau_E) e^{k\tau_E} k^{-3/4} P_\zeta(k)^{3/4} \Delta_\ell(k) j_\ell(kr) \end{aligned} \quad (57)$$

As anticipated, $Q[a]$ is of contact factorizable form (50) after replacing the (τ_E, r) double integral by a finite sum. This calculation generalizes to show that trispectra of the following types are contact factorizable:

1. Any ζ -trispectrum which is a product of functions $f(k_i)$ and any number of dot products of the form $(\mathbf{k}_i \cdot \mathbf{k}_j)$. The local trispectrum in Eq. (1) is an example. In this case we obtain a factorizable representation by applying the projection formula (37) and approximating the r integral by a finite sum.
2. Any trispectrum which arises from a local quartic operator in the inflationary action. We reduce to the previous case by writing the ζ -trispectrum as a time integral, and replacing the (τ_E, r) double integral by a finite sum.

In Appendix C, we work this out explicitly for the local, $(\dot{\sigma}^4)$, and $(\partial\sigma)^4$ trispectra. The resulting formulas (Eqs. (C2), (C5), (C11)) are useful for reference, and for numerical evaluation of trispectra in our analysis pipelines. In this appendix, we also present our scheme for generalizing from the scale invariant case (assumed above for simplicity) to the case of a power-law spectrum $P_\zeta(k) = A_\zeta k^{n_s - 4}$.

D. Exchange factorizability

As mentioned previously, there is another notion of factorizability for the trispectrum, ‘‘exchange factorizability’’, which arises from exchange of a light particle during inflation, and also leads to a computationally fast form for $Q[a]$. It would be interesting to explore the phenomenology and data analysis of exchange trispectra. For example, quasi-single field inflation [35, 44, 84, 85] should generate interesting continuous families of trispectra, as the mass of the exchanged particle and the type of cubic operator are varied. However in this paper, we will restrict attention to contact factorizable trispectra, leaving this generalization for future work. The main technical obstacle in generalizing the machinery of this paper to the exchange factorizable case is developing an analogue of the optimization algorithm in §VII. In this section, we simply give the definition of exchange factorizability and a few examples.

A CMB trispectrum is said to be exchange factorizable if the Q -symbol is given by:

$$Q_T[a] = \frac{1}{48} \sum_{I=1}^{N_1} \sum_{J=1}^{N_2} \sum_{\ell m} \mathcal{M}_\ell^{IJ} \left(\int d^2\hat{\mathbf{n}} ({}_{\alpha_I+\beta_I}Y_{\ell m}(\hat{\mathbf{n}}))^* \left(\sum_{\ell_1 m_1} A_{\ell_1}^I a_{\ell_1 m_1} ({}_{\alpha_I}Y_{\ell_1 m_1}(\hat{\mathbf{n}})) \right) \left(\sum_{\ell_2 m_2} B_{\ell_2}^I a_{\ell_2 m_2} ({}_{\beta_I}Y_{\ell_2 m_2}(\hat{\mathbf{n}})) \right) \right) \times \left(\int d^2\hat{\mathbf{n}}' ({}_{\gamma_J+\delta_J}Y_{\ell m}(\hat{\mathbf{n}}'))^* \left(\sum_{\ell_3 m_3} C_{\ell_3}^J a_{\ell_3 m_3} ({}_{\gamma_J}Y_{\ell_3 m_3}(\hat{\mathbf{n}}')) \right) \left(\sum_{\ell_4 m_4} D_{\ell_4}^J a_{\ell_4 m_4} ({}_{\delta_J}Y_{\ell_4 m_4}(\hat{\mathbf{n}}')) \right) \right)^* + \text{c.c.} \quad (58)$$

An exchange trispectrum is parametrized by integer spins $\alpha_I, \beta_I, \gamma_J, \delta_J$ and coefficient arrays $\mathcal{M}_\ell^{IJ}, A_\ell^I, B_\ell^I, C_\ell^J, D_\ell^J$, where $I = 1, \dots, N_1$ and $J = 1, \dots, N_2$. Note that contact factorizability can be viewed as the special case of exchange factorizability where $N_1 = N_2$ and $\mathcal{M}_\ell^{IJ} = \delta_{IJ}$ (with no ℓ dependence), so that the outer ℓ -sum gives a delta function $\delta^2(\hat{\mathbf{n}} - \hat{\mathbf{n}}')$. It is easy to see from the definition (58) that $Q_T[a]$ can be computed efficiently (more precisely, with cost $\mathcal{O}(N_1 \ell_{\max}^3 + N_2 \ell_{\max}^3 + N_1 N_2 \ell_{\max}^2)$) by an appropriate sequence of fast spherical harmonic transforms.

The canonical example of an exchange trispectrum is the τ_{NL} -trispectrum, defined previously in Eq. (3). To show that it is exchange factorizable, we first rewrite the ζ -trispectrum as:

$$\langle \zeta_{\mathbf{k}_1} \zeta_{\mathbf{k}_2} \zeta_{\mathbf{k}_3} \zeta_{\mathbf{k}_4} \rangle = \tau_{NL} \int \frac{d^3 \mathbf{q}}{(2\pi)^3} P_\zeta(q) P_\zeta(k_2) P_\zeta(k_4) (2\pi)^6 \delta^3(\mathbf{k}_1 + \mathbf{k}_2 + \mathbf{q}) \delta^3(\mathbf{k}_3 + \mathbf{k}_4 - \mathbf{q}) + (11 \text{ perm.}) \quad (59)$$

Following the calculation in the last section, we plug into the 3D \rightarrow 2D projection formula (37), Rayleigh expand both delta functions, and do the angular q and k -integrals. When the dust settles we get:

$$\begin{aligned} Q_T[a] = & \frac{\tau_{NL}}{2} \int d^3 \mathbf{r} d^3 \mathbf{r}' \left(\int \frac{2q^2 dq}{\pi} \sum_{\ell m} j_\ell(qr) j_\ell(qr') P_\zeta(q) Y_{\ell m}^*(\hat{\mathbf{r}}) Y_{\ell m}(\hat{\mathbf{r}}') \right) \\ & \times \left(\int \frac{2k_1^2 dk_1}{\pi} \sum_{\ell_1 m_1} j_{\ell_1}(k_1 r) \Delta_{\ell_1}(k_1) a_{\ell_1 m_1} Y_{\ell_1 m_1}(\hat{\mathbf{r}}) \right) \\ & \times \left(\int \frac{2k_2^2 dk_2}{\pi} \sum_{\ell_2 m_2} j_{\ell_2}(k_2 r) \Delta_{\ell_2}(k_2) P_\zeta(k_2) a_{\ell_2 m_2} Y_{\ell_2 m_2}(\hat{\mathbf{r}}) \right) \\ & \times \left(\int \frac{2k_3^2 dk_3}{\pi} \sum_{\ell_3 m_3} j_{\ell_3}(k_3 r') \Delta_{\ell_3}(k_3) a_{\ell_3 m_3} Y_{\ell_3 m_3}(\hat{\mathbf{r}}') \right) \\ & \times \left(\int \frac{2k_4^2 dk_4}{\pi} \sum_{\ell_4 m_4} j_{\ell_4}(k_4 r') \Delta_{\ell_4}(k_4) P_\zeta(k_4) a_{\ell_4 m_4} Y_{\ell_4 m_4}(\hat{\mathbf{r}}') \right) \end{aligned} \quad (60)$$

Using the standard notation [3, 86]:

$$\begin{aligned} \alpha_\ell(r) &= \frac{5}{3} \int \frac{2k^2 dk}{\pi} \Delta_\ell(k) j_\ell(kr) \\ \beta_\ell(r) &= \frac{3}{5} \int \frac{2k^2 dk}{\pi} \Delta_\ell(k) P_\zeta(k) j_\ell(kr) \\ F_\ell(r, r') &= \int \frac{2q^2 dq}{\pi} j_\ell(qr) j_\ell(qr') P_\zeta(q) \end{aligned} \quad (61)$$

we can write this in the form:

$$\begin{aligned} Q_T[a] = & \frac{\tau_{NL}}{2} \int r^2 dr \int r'^2 dr' \sum_{\ell m} F_\ell(r, r') \\ & \times \left(\int d^2 \hat{\mathbf{n}} Y_{\ell m}^*(\hat{\mathbf{n}}) \left(\sum_{\ell_1 m_1} \alpha_{\ell_1}(r) a_{\ell_1 m_1} Y_{\ell_1 m_1}(\hat{\mathbf{r}}) \right) \left(\sum_{\ell_2 m_2} \beta_{\ell_2}(r) a_{\ell_2 m_2} Y_{\ell_2 m_2}(\hat{\mathbf{r}}) \right) \right) \\ & \times \left(\int d^2 \hat{\mathbf{n}}' Y_{\ell m}^*(\hat{\mathbf{n}}') \left(\sum_{\ell_3 m_3} \alpha_{\ell_3}(r') a_{\ell_3 m_3} Y_{\ell_3 m_3}(\hat{\mathbf{r}}') \right) \left(\sum_{\ell_4 m_4} \beta_{\ell_4}(r') a_{\ell_4 m_4} Y_{\ell_4 m_4}(\hat{\mathbf{r}}') \right) \right)^* \end{aligned} \quad (62)$$

Comparing this expression with the definition (58), we see that the τ_{NL} trispectrum is exchange factorizable. This calculation generalizes to show that trispectra of the following types are exchange factorizable:

1. Any ζ -trispectrum which is a product of functions $f(k_i)$, any number of dot products $(\mathbf{k}_i \cdot \mathbf{k}_j)$, and one factor of the form $f(|\mathbf{k}_1 + \mathbf{k}_2|)$.
2. Any ζ -trispectrum generated by an ‘‘exchange’’ diagram of the type shown in the right side of Eq. (48).

Although our definition of exchange factorizability was constructed with inflationary trispectra in mind, there are also interesting non-primordial examples, for example gravitational lensing. The lensing trispectrum $T_{m_1 m_2 m_3 m_4}^{\ell_1 \ell_2 \ell_3 \ell_4}$ can

found in Eq. (76) of [78]. Plugging this into the definition (27) of $Q[a]$, we get the following expression for $Q_T[a]$:

$$\begin{aligned}
Q_T[a] = & \frac{1}{8} \sum_{s=\pm 1} \sum_{s'=\pm 1} \sum_{\ell m} \ell(\ell+1) C_\ell^{\phi\phi} \\
& \times \left(\int ({}_s Y_{\ell m})^* \left(\sum_{\ell_1 m_1} a_{\ell_1 m_1} Y_{\ell_1 m_1} \right) \left(\sum_{\ell_2 m_2} \sqrt{\ell_2(\ell_2+1)} C_{\ell_2}^{TT} a_{\ell_2 m_2} ({}_s Y_{\ell_2 m_2}) \right) \right) \\
& \times \left(\int ({}_{s'} Y_{\ell m})^* \left(\sum_{\ell_3 m_3} a_{\ell_3 m_3} Y_{\ell_3 m_3} \right) \left(\sum_{\ell_4 m_4} \sqrt{\ell_4(\ell_4+1)} C_{\ell_4}^{TT} a_{\ell_4 m_4} ({}_{s'} Y_{\ell_4 m_4}) \right) \right)^* \quad (63)
\end{aligned}$$

Comparing with the definition (58), we see that the CMB lensing trispectrum is exchange factorizable. In this case, there is no obstacle to applying the machinery in this paper (since there are only a few terms in the trispectrum, we do not need an optimization algorithm). The pipelines we will develop in §IX could be used to give an optimal analysis of CMB lensing. Such an analysis would be qualitatively similar to other lens reconstruction analyses (e.g. [28, 29, 87]) but different in its approach to minimizing bias due to errors in modeling the two-point function.

VI. FISHER MATRIX ALGORITHMS

Consider an ideal CMB experiment with full sky coverage and isotropic noise. Such an experiment is completely specified by its noise power spectrum N_ℓ . Given angular trispectra T_1, \dots, T_N , the N -by- N Fisher matrix is defined by

$$F_{ij} = \frac{1}{4!} \sum_{\ell_i m_i} \frac{(T_i)_{m_1 m_2 m_3 m_4}^{\ell_1 \ell_2 \ell_3 \ell_4} (T_j)_{m_1 m_2 m_3 m_4}^{\prime \ell_1 \ell_2 \ell_3 \ell_4}}{(C_{\ell_1} + N_{\ell_1})(C_{\ell_2} + N_{\ell_2})(C_{\ell_3} + N_{\ell_3})(C_{\ell_4} + N_{\ell_4})} \quad (64)$$

and is interpreted as follows. If the CMB trispectrum is assumed to be a linear combination $T = \sum_i g_{NL}^i T_i$ of the trispectra T_i , and the coefficients g_{NL}^i are jointly estimated using optimal estimators, then the estimator covariance is the inverse Fisher matrix:

$$\text{Cov}(g_{NL}^i, g_{NL}^j) = (F^{-1})_{ij} \quad (65)$$

The Fisher matrix is a powerful tool for forecasting and analysis of parameter degeneracies.⁶ It will also play a central role in the trispectrum optimization algorithm which we will give in §VII.

Computing the Fisher matrix directly from the definition (64) has computational cost $\mathcal{O}(\ell_{\text{max}}^7)$ and is usually computationally prohibitive. In this section we will construct fast algorithms.

A. Monte Carlo Fisher matrix algorithm

A very simple fast algorithm for estimating the Fisher matrix is to use the following Monte Carlo procedure:

$$F(T, T') = \left\langle \sum_{\ell m} \frac{(\partial_{\ell m} Q_T[\tilde{a}])^* (\partial_{\ell m} Q_{T'}[\tilde{a}])}{C_\ell + N_\ell} \right\rangle_{\tilde{a}} \quad (66)$$

where $\langle \cdot \rangle_{\tilde{a}}$ denotes an expectation value over Gaussian random fields $\tilde{a}_{\ell m}$ with power spectrum $1/(C_\ell + N_\ell)$ (not power spectrum $C_\ell + N_\ell$). The Monte Carlo error on the Fisher matrix is proportional to $1/\sqrt{N_{\text{mc}}}$, where N_{mc} is the number of random realizations. In practice we find that the proportionality coefficient is very favorable; even one Monte Carlo realization is enough to approximate the Fisher matrix to $\approx 10\%$ percent for the local trispectrum, or a few percent for the trispectra generated by one of the quartic operators $\dot{\sigma}^4$, $\dot{\sigma}^2(\partial_i \sigma)^2$, or $(\partial_i \sigma)^2(\partial_j \sigma)^2$.

The Monte Carlo algorithm in Eq. (66) may appear to be more complicated than necessary, since one can give a simpler Monte Carlo algorithm by simply estimating the variance of the all-sky optimal estimator for the trispectrum

⁶ Of course, the assumptions of full sky coverage and isotropic noise will not be satisfied for a real experiment, but it is usually a good approximation to approximate the noise as isotropic, and account for sky coverage by scaling $F \rightarrow f_{\text{sky}} F$.

T . However, the fractional Monte Carlo error of this simpler algorithm would be by the “standard” $\sqrt{2/N_{\text{mc}}}$, so it takes many random realizations to obtain a useful estimate of the Fisher matrix. For this reason we always use the algorithm (66) to estimate the Fisher matrix by Monte Carlo.

This is our first example of a phenomenon which will recur throughout the paper: there is an “obvious” Monte Carlo scheme which requires a large number of Monte Carlos, and an alternate scheme which is significantly faster. This phenomenon also occurs in the bispectrum context (e.g. Fig. 6 of [21]), where it was referred to as “fast MC”. We will see more examples shortly.

B. Exact Fisher matrix algorithm for contact factorizable trispectra

In this section, we will present an exact (i.e. non Monte Carlo based) Fisher matrix algorithm, which assumes contact factorizable trispectra. This is less generality than the Monte Carlo algorithm from the preceding section, which only requires a fast algorithm for evaluating the Q -symbol.

Let T be contact factorizable with spins $\alpha_I, \beta_I, \gamma_I, \delta_I$ and coefficients $A_{I\ell}, B_{I\ell}, C_{I\ell}, D_{I\ell}$ with $I = 1, 2, \dots, N_{\text{fact}}$. Likewise let T' be contact factorizable with spins $\alpha'_J, \beta'_J, \gamma'_J, \delta'_J$ and coefficients $A'_{J\ell}, B'_{J\ell}, C'_{J\ell}, D'_{J\ell}$ with $J = 1, 2, \dots, N'_{\text{fact}}$.

To obtain an exact expression for $F(T, T')$, we calculate as follows. First write:

$$F(T, T') = \left\langle Q_T[\tilde{a}] Q_{T'}[\tilde{a}] \right\rangle_{\text{f.c.}} \quad (67)$$

where \tilde{a} is a Gaussian random field with power spectrum $1/(C_\ell + N_\ell)$ and $\langle \cdot \rangle_{\text{f.c.}}$ denotes the fully connected part of the expectation value, i.e. the sum over Wick contractions in which all four contractions connect a factor of $Q_T[\tilde{a}]$ to a factor of $Q_{T'}[\tilde{a}]$. We write the Q -symbols in the abbreviated form:

$$\begin{aligned} Q_T[\tilde{a}] &= \frac{1}{48} \sum_{I=1}^{N_{\text{fact}}} \int d^2 \hat{\mathbf{n}} M_{\alpha_I}^{A_I}(\hat{\mathbf{n}}) M_{\beta_I}^{B_I}(\hat{\mathbf{n}}) M_{\gamma_I}^{C_I}(\hat{\mathbf{n}}) M_{\delta_I}^{D_I}(\hat{\mathbf{n}}) + \text{c.c.} \\ Q_{T'}[\tilde{a}] &= \frac{1}{48} \sum_{J=1}^{N'_{\text{fact}}} \int d^2 \hat{\mathbf{n}}' M_{\alpha'_J}^{A'_J}(\hat{\mathbf{n}}') M_{\beta'_J}^{B'_J}(\hat{\mathbf{n}}') M_{\gamma'_J}^{C'_J}(\hat{\mathbf{n}}') M_{\delta'_J}^{D'_J}(\hat{\mathbf{n}}') + \text{c.c.} \end{aligned} \quad (68)$$

where we have introduced the following notation. If $X = X_\ell$ is any ℓ -dependent quantity and s is an integer spin, then M_s^X is the spin- s map defined by

$$M_s^X(\hat{\mathbf{n}}) = \sum_{\ell m} X_\ell \tilde{a}_{\ell m} ({}_s Y_{\ell m}(\hat{\mathbf{n}})) \quad (69)$$

We plug the Q -symbols in Eq. (68) into the the expression (67) for $F(T, T')$ and expand the result as a sum of Wick contractions. The contraction between two M fields or their complex conjugates is easy to calculate using the sum rule (A8) in Appendix A:

$$\overline{M_s^X(\hat{\mathbf{n}})} M_{s'}^{X'}(\hat{\mathbf{n}}') = (-1)^s \zeta_{ss'}^{XX'-}(\theta) \quad \overline{M_s^X(\hat{\mathbf{n}})} M_{s'}^{X'}(\hat{\mathbf{n}}')^* = (-1)^s \zeta_{ss'}^{XX'+}(\theta) \quad (70)$$

where $\theta = \cos^{-1}(\hat{\mathbf{n}} \cdot \hat{\mathbf{n}}')$ is the angle between $\hat{\mathbf{n}}, \hat{\mathbf{n}}'$ and we have defined correlation functions

$$\zeta_{ss'}^{XX'\pm}(\theta) = (\pm 1)^{s'} \sum_{\ell} \frac{2\ell + 1}{4\pi} \frac{X_\ell X'_\ell}{C_\ell + N_\ell} d_{s, \mp s'}^\ell(\theta) \quad (71)$$

When the dust settles, we get the following explicit formula for $F(T, T')$:

$$F(T, T') = \frac{\pi^2}{144} \sum_{I=1}^{N_{\text{fact}}} \sum_{J=1}^{N'_{\text{fact}}} \sum_{\sigma=+,-} \int_{-1}^1 d(\cos \theta) \left(\zeta_{\alpha_I \alpha'_J}^{A_I A'_J \sigma}(\theta) \zeta_{\beta_I \beta'_J}^{B_I B'_J \sigma}(\theta) \zeta_{\gamma_I \gamma'_J}^{C_I C'_J \sigma}(\theta) \zeta_{\delta_I \delta'_J}^{D_I D'_J \sigma}(\theta) + 23 \text{ perm.} \right) \quad (72)$$

The integral can be evaluated exactly using Gauss-Legendre quadrature with $(2\ell_{\text{max}} + 1)$ points, since the integrand is a polynomial of degree $4\ell_{\text{max}}$. For each quadrature point θ , one ζ -function value $\zeta(\theta)$ can be computed with cost $\mathcal{O}(\ell_{\text{max}})$ using the recursion (A3). Thus the computational cost of computing $F(T, T')$ is $\mathcal{O}(N_{\text{fact}} N'_{\text{fact}} \ell_{\text{max}}^2)$.

Let us compare the computational cost of the exact algorithm in this section with the Monte Carlo algorithm from the previous section (assuming contact factorizable trispectra). Suppose we have N_{tr} total trispectra (i.e. the Fisher matrix being computed is N_{tr} -by- N_{tr}) and each trispectrum has N_{fact} factorizable terms. The exact algorithm has cost $\mathcal{O}(N_{\text{tr}}^2 N_{\text{fact}}^2 \ell_{\text{max}}^2)$, and the Monte Carlo algorithm has cost $\mathcal{O}(N_{\text{mc}} N_{\text{tr}} N_{\text{fact}} \ell_{\text{max}}^3 + N_{\text{mc}} N_{\text{tr}}^2 \ell_{\text{max}}^2)$.

Most interesting trispectra have factorizable representations with at most a few hundred terms (see Table I below), and the exact algorithm is actually faster due to the smaller power of ℓ_{max} . The Monte Carlo algorithm is useful in situations where the total number of factorizable terms is very large. For an example, see Appendix D, where we describe a Fisher matrix based convergence test on numerical calculation of trispectra. The Monte Carlo algorithm is also the only option for exchange factorizable trispectra. For example, we will use the Monte Carlo Fisher matrix to compute the lensing bias to our WMAP g_{NL} estimates (see Eq. (93) below).

VII. OPTIMIZATION ALGORITHM FOR CONTACT FACTORIZABLE TRISPECTRA

Consider the trispectrum generated by a quartic operator such as $\dot{\sigma}^4$. So far, we have proposed a scheme for representing the trispectrum in contact factorizable form (50), and shown that this representation reduces the computational cost of data analysis from $\mathcal{O}(\ell_{\text{max}}^7)$ to $\mathcal{O}(N_{\text{fact}} \ell_{\text{max}}^3)$, by providing a fast algorithm for computing the Q -symbol $Q[a]$. However, this is not quite enough to bring the computational cost fully under control, since the number of terms N_{fact} in the factorizable representation can be very large.

For example, consider the trispectrum generated by the quartic operator $\dot{\sigma}^2(\partial\sigma)^2$. To represent it in factorizable form, we must approximate the double (τ_E, r) integral in Eq. (56) by a finite sum. To accurately approximate the detailed (ℓ, m) dependence of the trispectrum, a huge number of sampling points in the (τ_E, r) plane is required. This issue is studied in detail in Appendix D. As explained there, our sampling scheme has the property that the finite-sampled trispectrum approximates the exact trispectrum in a controlled sense: there is an end-to-end convergence test which shows that the two are nearly equal in the metric defined by the Fisher matrix. However, this requires many sampling points in the (τ_E, r) plane, e.g. for the operator $\dot{\sigma}^2(\partial\sigma)^2$ and WMAP noise levels, we find that 31763 sampling points are needed!

Fortunately, there is an optimization algorithm, first proposed for the bispectrum in [21], which can dramatically reduce the number of terms in the factorizable representation. The input to the algorithm is a trispectrum which has been represented in contact factorizable form with a large number N_{in} of terms. We write:

$$T_{\text{in}} = \sum_{I=1}^{N_{\text{in}}} T_I \quad (73)$$

where T_I is the I -th term in the factorizable representation. The output is an ‘‘optimized’’ representation obtained by linearly combining a small subset of terms in the input representation. Formally:

$$T_{\text{out}} = \sum_{J=1}^{N_{\text{out}}} w_J T_{I_J} \quad (74)$$

with the subset $\{T_{I_1}, T_{I_2}, \dots\}$ of terms and weights w_J determined by the optimization algorithm.

The first step in the optimization algorithm is to compute the N_{in} -by- N_{in} Fisher matrix $F_{IJ} = F(T_I, T_J)$ of individual terms in the input representation. We use the exact Fisher matrix algorithm from §VIB to compute F_{IJ} .⁷ Once this matrix has been computed, the optimized representation T_{out} can then be computed using a purely formal linear algebra procedure described in §V.A of [21]. (This procedure was developed for purposes of optimizing the bispectrum, but the Fisher matrix contains all the information needed for the optimization, and once it has been computed it no longer matters whether the underlying objects are bispectra or trispectra.) The optimization algorithm guarantees that the input and output trispectra are nearly equal, in the sense that

$$F(T_{\text{in}} - T_{\text{out}}, T_{\text{in}} - T_{\text{out}}) < 10^{-5} F(T_{\text{in}}, T_{\text{in}}) \quad (75)$$

where $F(T, T')$ denotes the Fisher matrix element. This definition of ‘‘nearly equal’’ means that the two trispectra cannot be distinguished observationally with statistical significance. Because the Fisher matrix depends on the noise power spectrum, the optimized trispectrum depends weakly on the noise properties of the experiment being considered.

⁷ In this case, the exact Fisher matrix algorithm has computational cost $\mathcal{O}(N_{\text{in}}^2 \ell_{\text{max}}^2)$, whereas the Monte Carlo Fisher matrix algorithm from §VIA has cost $\mathcal{O}(N_{\text{mc}} N_{\text{in}} \ell_{\text{max}}^3 + N_{\text{mc}} N_{\text{in}}^2 \ell_{\text{max}}^2)$. The exact algorithm turns out to be faster even for modest values of N_{mc} .

There is one more wrinkle: for the large input representations considered here with $N_{\text{in}} \gtrsim 10^4$, computing the Fisher matrix $F_{I,J}$ is a computational bottleneck. To get around this problem, we use a two-stage optimization algorithm as follows. We divide the input representation into M “chunks” of size (N_{in}/M) , where typically $M = 16$ or 32, and optimize each chunk separately. (Note that the total cost of optimizing all chunks is less than the cost of optimizing their sum, since the exact Fisher matrix algorithm scales as N_{fact}^2 , not N_{fact} .) We then combine the optimized chunks to obtain a semi-optimized representation of the input bispectrum, and do a second pass of the optimization algorithm to obtain the final optimized representation.

In Table I, we show results of applying the optimization algorithm to the g_{NL}^{loc} , $\dot{\sigma}^4$, $\dot{\sigma}^2(\partial\sigma)^2$, and $(\partial\sigma)^4$ trispectra. It is seen that the optimization algorithm results in a dramatic reduction in the size of the factorizable representation. The optimized representations will be used throughout the rest of the paper.

Trispectrum	N_{in}	N_{out}
g_{NL}^{loc}	960	16
$\dot{\sigma}^4$	31763	52
$\dot{\sigma}^2(\partial\sigma)^2$	63526	110
$(\partial\sigma)^4$	95289	141

TABLE I: Number of factorizable terms N_{in} needed to represent each trispectrum by “brute-force” replacement of integrals by finite sums (see Appendix D for details), and number of terms N_{out} obtained after running the optimization algorithm with WMAP noise levels.

VIII. FISHER MATRIX ANALYSIS OF THE TRISPECTRA $\dot{\sigma}^4$, $\dot{\sigma}^2(\partial\sigma)^2$, AND $(\partial\sigma)^4$

In this section, we will study correlations between the trispectra $\{\dot{\sigma}^4, \dot{\sigma}^2(\partial\sigma)^2, (\partial\sigma)^4\}$, using the CMB Fisher matrix studied in §VI.

We note in passing that for primordial trispectra, there is an alternate, simpler choice of Fisher matrix defined by:

$$F(T_1, T_2) = \int \frac{d^3\mathbf{k}_1 d^3\mathbf{k}_2 d^3\mathbf{k}_3 d^3\mathbf{k}_4}{(2\pi)^{12}} \frac{\langle \zeta_{\mathbf{k}_1} \zeta_{\mathbf{k}_2} \zeta_{\mathbf{k}_3} \zeta_{\mathbf{k}_4} \rangle'_1}{P_\zeta(k_1)P_\zeta(k_2)P_\zeta(k_3)P_\zeta(k_4)} \frac{\langle \zeta_{\mathbf{k}_1} \zeta_{\mathbf{k}_2} \zeta_{\mathbf{k}_3} \zeta_{\mathbf{k}_4} \rangle'_2}{(2\pi)^3 \delta^3 \left(\sum \mathbf{k}_i \right)} \quad (76)$$

This is the appropriate definition for an observer who sees all ζ -modes in a 3D volume (as opposed an observer who sees all CMB modes on a 2D sky). In the bispectrum case, the 3D Fisher matrix and the 2D CMB Fisher matrix tend to give nearly identical results in practice. However, this need not be so for the trispectrum, since 3D→2D projection actually reduces the dimensionality of the parameter space. The 3D ζ -bispectrum and the 2D CMB bispectrum are both functions of three parameters (assuming translation and rotation invariance in the 3D case, and rotation invariance in the 2D case). In contrast, the 3D ζ -trispectrum is a function of six parameters, but the 2D CMB trispectrum is a function of only five. As a point of mathematical principle, this implies that there must exist examples of ζ -trispectra which are weakly correlated in 3D, but become highly correlated when projected to the CMB. For this reason, we have used the CMB Fisher matrix throughout this section rather than the simpler 3D Fisher matrix (76), but we actually find that the two Fisher matrices agree well for the trispectra under consideration.

Let us recall the Fisher matrix analysis for the bispectrum which gives rise to the parameters f_{NL}^{eq} and f_{NL}^{orth} [6]. There are two cubic operators to consider, $\hat{\pi}^3$ and $\hat{\pi}(\partial\pi)^2$. These generate bispectra which are nonidentical, but correlated at the ≈ 0.9 level. This level of correlation is not so large that the two operators can be treated as indistinguishable, but is large enough that orthogonalization is convenient [6]. We therefore apply a linear transformation in the parameter space $(\hat{\pi}^3, \hat{\pi}(\partial\pi)^2)$ to define (approximately) decorrelated observables f_{NL}^{eq} , f_{NL}^{orth} .

Analogously, for the trispectrum, the three quartic operators $\{\dot{\sigma}^4, \dot{\sigma}^2(\partial\sigma)^2, (\partial\sigma)^4\}$ generate three distinct trispectra. Using the exact Fisher matrix algorithm from §VIB, the correlation matrix between these trispectra is found to be:

$$\begin{pmatrix} 1 & 0.9484 & 0.7558 \\ 0.9484 & 1 & 0.9083 \\ 0.7558 & 0.9083 & 1 \end{pmatrix} \quad (77)$$

From this Fisher matrix, it can be shown that any of the three trispectra is highly correlated to a linear combination of the other two. For example, the trispectrum $\dot{\sigma}^2(\partial\sigma)^2$ is 99.2% correlated to a linear combination of $\dot{\sigma}^4$ and $(\partial\sigma)^4$.

Therefore, we will not treat $\dot{\sigma}^2(\partial\sigma)^2$ as a new trispectrum which is independent of the other two. More concretely, we can convert $g_{NL}^{\dot{\sigma}^2(\partial\sigma)^2}$ into the following effective values of $g_{NL}^{\dot{\sigma}^4}$ and $g_{NL}^{(\partial\sigma)^4}$:

$$(g_{NL}^{\dot{\sigma}^4})_{\text{eff}} = 0.620g_{NL}^{\dot{\sigma}^2(\partial\sigma)^2} \quad (g_{NL}^{(\partial\sigma)^4})_{\text{eff}} = 0.0936g_{NL}^{\dot{\sigma}^2(\partial\sigma)^2} \quad (78)$$

Note that we have choose our trispectrum basis to simply be the coefficients of the operators $\dot{\sigma}^4$ and $(\partial\sigma)^4$, rather than orthogonalizing as in the case of the bispectrum. This somewhat simplifies the analysis and interpretation, but it should be kept in mind that the two operators are $\approx 75\%$ correlated.

The local trispectra g_{NL}^{loc} is not particularly correlated to any of the quartic operator trispectra $(\dot{\sigma}^4, \dot{\sigma}^2(\partial\sigma)^2, (\partial\sigma)^4)$. This can be understood by noting that the local trispectrum gets most of its signal-to-noise from the squeezed limit $k_1 \ll \min(k_2, k_3, k_4)$, whereas the other trispectra vanish in the squeezed limit.

Throughout the preceding Fisher matrix analysis, we have used WMAP noise levels. If we use Planck noise levels instead, the results are qualitatively unchanged but the numerics are slightly different. The correlation matrix between the $\dot{\sigma}^4$, $\dot{\sigma}^2(\partial_i\sigma)^2$, $(\partial_i\sigma)^2(\partial_j\sigma)^2$, and $(\partial_i\sigma)^2(\partial_j\sigma)^2$ trispectra is:

$$\begin{pmatrix} 1 & 0.9113 & 0.6142 \\ 0.9113 & 1 & 0.8572 \\ 0.6142 & 0.8572 & 1 \end{pmatrix} \quad (\text{Planck noise}) \quad (79)$$

The $\dot{\sigma}^2(\partial_i\sigma)^2$ shape is 98.6% correlated to a linear combination of the other two shapes. The coefficients which convert $g_{NL}^{\dot{\sigma}^2(\partial\sigma)^2}$ to effective values of $g_{NL}^{\dot{\sigma}^4}$ and $g_{NL}^{(\partial\sigma)^4}$ are:

$$(g_{NL}^{\dot{\sigma}^4})_{\text{eff}} = 0.597g_{NL}^{\dot{\sigma}^2(\partial\sigma)^2} \quad (g_{NL}^{(\partial\sigma)^4})_{\text{eff}} = 0.0914g_{NL}^{\dot{\sigma}^2(\partial\sigma)^2} \quad (\text{Planck noise}) \quad (80)$$

IX. ANALYSIS PIPELINES

In this section, we develop an analysis pipeline for estimating the amplitude of a trispectrum T for a realistic CMB experiment. We will actually develop two analysis pipelines which are appropriate for different sets of assumptions.

In some experiments, it is computationally feasible to multiply a harmonic-space map by the operator C^{-1} which appears in the optimal trispectrum estimator (Eq. (24)). For example, this is possible for WMAP, since the noise model is simple: it is an excellent approximation to treat the noise covariance as diagonal in the pixel domain. In §IX A below, we develop an optimal pipeline for such experiments.

In other experiments, it is infeasible to multiply a map by C^{-1} , either because this is too computationally slow, or because the noise model is too complicated. The case we have in mind is Planck, although we will not attempt a Planck trispectrum analysis in this paper. The foreground-cleaned maps used for non-Gaussianity analysis by the Planck collaboration [9] have a noise covariance which in principle is determined precisely by the scan strategy, timestream noise properties, and foreground cleaning method. However, pixel-pixel correlations are important, exact multiplication of a map by N^{-1} is likely to be as expensive as full map-making, and multiplication by C^{-1} (requiring iterated multiplication by N^{-1}) is likely prohibitive. Fortunately, we can still proceed by implementing a filter which approximates but is not precisely equal to C^{-1} . Another feature of the Planck analysis is that making Monte Carlo simulations of foreground cleaned maps is expensive. A common set of Monte Carlo simulations is shared between the Planck trispectrum analysis, bispectrum analysis, and other analyses, but it is impractical to make new simulations specifically for the trispectrum pipeline.

With these considerations in mind, in §IX B below, we propose a ‘‘pure MC’’ pipeline which compares the trispectrum of the data to the trispectrum of an external set of Monte Carlo simulations, using a filter which is not necessarily equal to C^{-1} .

An important property of the pure MC pipeline is that it does not assume that the simulations are Gaussian. For example, we might use lensed CMB simulations, which have a nonzero trispectrum. In this case, the pure MC pipeline is constructed so that it estimates the trispectrum of the data in excess of the simulations, i.e. lensing bias will automatically be subtracted from the estimated trispectrum.

We have not worked out how to remove lensing bias in the optimal pipeline, since our immediate goal is to use the optimal pipeline to analyze WMAP, where lensing is a small effect. In cases where lensing bias is small, we can accurately approximate it using a Fisher matrix based estimate; see discussion near Eq. (93) below.

In a case where C^{-1} is affordable but lensing bias is large, currently our only way of obtaining optimal error bars with reliable lensing bias subtraction would be to run the pure MC pipeline with C^{-1} filtering rather than running the optimal pipeline. This has one disadvantage: the optimal pipeline is much faster to converge than the pure MC pipeline, since we can use the assumption of Gaussian simulations to give a ‘‘fast MC’’ algorithm. The ultimate

pipeline would combine the fast convergence of the optimal pipeline and bias subtraction properties of the pure MC pipeline, but we defer construction of such a pipeline to future work.

A. Optimal pipeline

In this section we describe our first pipeline: an optimal pipeline which can be applied to experiments where C^{-1} filtering is practical. Although more general, this pipeline was developed with WMAP in mind. Let us state our assumptions explicitly:

1. The observed CMB $a_{\ell m} = s_{\ell m} + n_{\ell m}$ is the sum of the true sky signal $s_{\ell m}$ and a Gaussian noise realization $n_{\ell m}$. (Our convention here is that $a_{\ell m}$ denotes the beam-deconvolved map.)
2. Given a harmonic-space map $b_{\ell m}$, computing $(C^{-1}b)_{\ell m}$ is computationally feasible.
3. It is also computationally feasible to randomly generate a signal + noise realization, i.e. a Gaussian random map $b_{\ell m}$ with covariance matrix C .

Throughout this section we will use the abbreviated notation

$$\tilde{a}_{\ell m} = C_{\ell m, \ell' m'}^{-1} a_{\ell' m'} \quad (81)$$

As shown previously (Eq. (28)), the optimal estimator is $\hat{\mathcal{E}}[a] = (1/F)\hat{\mathcal{E}}_0[a]$, where $\hat{\mathcal{E}}_0[a]$ can be computed as a Monte Carlo average over Gaussian signal+noise realizations b :

$$\hat{\mathcal{E}}_0[a] = \left\langle Q[\tilde{a}, \tilde{a}, \tilde{a}] - 6Q[\tilde{a}, \tilde{a}, \tilde{b}] + Q[\tilde{b}, \tilde{b}, \tilde{b}] \right\rangle_b \quad (82)$$

The quantity F was defined previously in Eq. (25). It determines both the normalization of the estimator and its variance. More precisely, $\text{Var}(\hat{\mathcal{E}}) = 1/F$ or equivalently $\text{Var}(\hat{\mathcal{E}}_0) = F$.

Since evaluating $\hat{\mathcal{E}}_0$ by Monte Carlo is straightforward given our assumptions, the only issue in the optimal pipeline is an algorithm for computing F . This involves some nontrivial computational challenges, as we now explain.

Since $F = \text{Var}(\hat{\mathcal{E}}_0)$, one natural approach is to evaluate $\hat{\mathcal{E}}_0$ on an ensemble of Gaussian simulations and estimate the variance to get F . Unfortunately, if implemented naively, the computational cost of this approach is $\mathcal{O}(N_{\text{mc}}^2)$, not $\mathcal{O}(N_{\text{mc}})$! This is due to a curious property of the estimator (82): if we want to evaluate the estimator on a new realization a , we must recompute the Monte Carlo average $\langle Q[\tilde{a}, \tilde{a}, \tilde{b}] \rangle$ “from scratch” by looping over random realizations b with computational cost $\mathcal{O}(N_{\text{mc}})$.

One idea for reducing the computational cost from $\mathcal{O}(N_{\text{mc}}^2)$ to $\mathcal{O}(N_{\text{mc}})$ is to group Monte Carlo simulations into pairs $(b_1, b'_1), (b_2, b'_2), \dots$. We then express F as a Monte Carlo average involving only expressions which can be computed from a single pair, for example $Q[b_i, b_i, b_i, b_i]$ or $Q[b_i, b_i, b'_i, b'_i]$, but not $Q[b_i, b_i, b_j, b_j]$.

A second, more technical idea for reducing computational cost is to use Monte Carlo averages involving (∂Q) , which converge much faster than averages involving Q . This was noted previously in our discussion of the isotropic all-sky Fisher matrix (§VIA).

Combining these ideas, we express F as the following Monte Carlo average over pairs (b, b') :

$$\begin{aligned} F = & \frac{1}{32} \left\langle (\partial_{\ell m} Q[\tilde{b}, \tilde{b}, \tilde{b}]) C_{\ell m, \ell' m'}^{-1} (\partial_{\ell' m'} Q[\tilde{b}, \tilde{b}, \tilde{b}]) + (\partial_{\ell m} Q[\tilde{b}', \tilde{b}', \tilde{b}']) C_{\ell m, \ell' m'}^{-1} (\partial_{\ell' m'} Q[\tilde{b}', \tilde{b}', \tilde{b}']) \right\rangle \\ & + \frac{9}{32} \left\langle (\partial_{\ell m} Q[\tilde{b}, \tilde{b}, \tilde{b}']) C_{\ell m, \ell' m'}^{-1} (\partial_{\ell' m'} Q[\tilde{b}, \tilde{b}, \tilde{b}']) + (\partial_{\ell m} Q[\tilde{b}, \tilde{b}', \tilde{b}']) C_{\ell m, \ell' m'}^{-1} (\partial_{\ell' m'} Q[\tilde{b}, \tilde{b}', \tilde{b}']) \right\rangle \\ & - \frac{3}{16} \left\langle (\partial_{\ell m} Q[\tilde{b}, \tilde{b}, \tilde{b}]) C_{\ell m, \ell' m'}^{-1} (\partial_{\ell' m'} Q[\tilde{b}, \tilde{b}', \tilde{b}']) + (\partial_{\ell m} Q[\tilde{b}', \tilde{b}', \tilde{b}']) C_{\ell m, \ell' m'}^{-1} (\partial_{\ell' m'} Q[\tilde{b}, \tilde{b}, \tilde{b}']) \right\rangle. \quad (83) \end{aligned}$$

The specific choice of coefficients $(1/32, 9/32, -3/16)$ is motivated in Appendix E.

It is sometimes useful to know the “error on the error”, i.e. the statistical error on our estimate of F due to the finite number of Monte Carlos. We estimate this straightforwardly, since F is an average over pairs (b, b') , so we can estimate its uncertainty from the scatter between pairs. The estimator for F given in Eq. (83) has been designed to minimize this scatter, and in practice we do not need many Monte Carlos to get convergence.

As previously mentioned, we emphasize that the optimal pipeline assumes Gaussian statistics and in particular does not subtract lensing bias. Note that simply using lensed simulations in the optimal estimator (82) does not correctly remove lensing bias. For WMAP the lensing bias is small, but in a case where it is large and must be subtracted accurately, then the only option is the pure MC pipeline which we present next.

B. Pure MC pipeline

We now describe our second pipeline, a pipeline which operates on an external ensemble of Monte Carlo simulations. We start by choosing a filter which can be applied to the data to produce a harmonic-space map $\tilde{a}_{\ell m}$. To obtain near-optimal statistical errors, the filter should be chosen to approximate C^{-1} filtering as closely as possible. For example, to analyze Planck data, we could use the same filtering used for the bispectrum analysis [9]: we start with foreground-cleaned maps in pixel space, inpaint the mask, transform to harmonic space, and multiply by $1/(C_\ell + N_\ell)$, where N_ℓ is a sky-averaged noise power spectrum. This filter is suboptimal in principle, since it is not precisely equal to C^{-1} , but has been shown to be near-optimal for Planck, at least for the bispectrum.

Let us state the assumptions of our “pure MC” pipeline:

1. The observed sky is specified as a filtered harmonic-space map $\tilde{a}_{\ell m}$, and we want to compare its trispectrum to a set of external simulations, also specified as filtered harmonic-space maps $\tilde{b}_{\ell m}^{(1)}, \tilde{b}_{\ell m}^{(2)}, \dots$. (In this section, we use tildes to denote any map which has been processed by the filter.)
2. The observed sky is a sum of signal and noise components $\tilde{a}_{\ell m} = \tilde{s}_{\ell m} + \tilde{n}_{\ell m}$ (and likewise for the simulations). The filtered signal $\tilde{s}_{\ell m}$ is related to the true CMB sky by a linear operator T , i.e. $\tilde{s}_{\ell m} = (Ts)_{\ell m}$, and the signal and noise are statistically independent.
3. For each simulation, we know the underlying CMB realization $s_{\ell m}$ which was used. An important feature of the pure MC pipeline is that we do not assume that either the CMB or noise realizations used in the simulations are Gaussian. If the simulations are non-Gaussian, then the trispectrum estimator will return an estimate of the trispectrum amplitude in excess of any trispectrum which is in the simulations. This is very convenient in practice. For example, if the CMB realizations may be lensed, and the noise realizations include residual foregrounds, then lensing and foreground contributions to the trispectrum will automatically be subtracted.
4. Given an arbitrary CMB map $b_{\ell m}$, there is a fast algorithm for computing $(Tb)_{\ell m}$. Typically this will involve convolving with a beam or instrumental response, taking the spherical transform to pixel space, then applying the same filter which was applied to the data.

Our pipeline will use an estimator of the form $\hat{\mathcal{E}}[\tilde{a}] = (1/F_N)\hat{\mathcal{E}}_0[\tilde{a}]$, where the unnormalized estimator is defined by the Monte Carlo average:

$$\hat{\mathcal{E}}_0[a] = Q[\tilde{a}, \tilde{a}, \tilde{a}, \tilde{a}] - 6 \left\langle Q[\tilde{a}, \tilde{a}, \tilde{b}, \tilde{b}] \right\rangle_b - \left\langle Q[\tilde{b}, \tilde{b}, \tilde{b}, \tilde{b}] \right\rangle_b + 6 \left\langle Q[\tilde{b}, \tilde{b}, \tilde{b}', \tilde{b}'] \right\rangle_{b,b'} \quad (84)$$

and the normalization F_N will be specified shortly (Eq. (85) below).

It is easy to verify two key properties of this estimator. First, its expectation value over the simulations vanishes: $\langle \hat{\mathcal{E}}_0[b] \rangle = 0$. This means that $\hat{\mathcal{E}}_0[a]$ measures the trispectrum of the data relative to the trispectrum of the simulations, as desired. Second, if the two-point function of the simulations does not perfectly match the two-point function of the data, due to slightly incorrect cosmological parameters or noise model, then the bias on $\hat{\mathcal{E}}_0$ will be second order. As shown previously in §III, this is an important property of the optimal estimator, and we would like to preserve it in our pure MC pipeline.

The last term in the estimator (84) is a double Monte Carlo average over pairs of simulations (b, b') . This is necessary because we are not assuming Gaussian simulations. If simulations were Gaussian, then we could use the relation $\langle Q[\tilde{b}, \tilde{b}, \tilde{b}, \tilde{b}] \rangle_b = 3 \langle Q[\tilde{b}, \tilde{b}, \tilde{b}', \tilde{b}'] \rangle_{b,b'}$ to rewrite the last term as an average over single simulations b . Note that if we assumed Gaussianity, and also assumed optimal filtering (i.e. $\tilde{a} = C^{-1}a$) then the estimator $\hat{\mathcal{E}}_0$ would reduce to the optimal estimator studied previously.

In our pure MC pipeline, we would like to compute the unnormalized estimator $\hat{\mathcal{E}}_0[a]$, the estimator normalization F_N , and the variance $F_V = \text{Var}(\hat{\mathcal{E}}_0)$ by Monte Carlo. We would also like to compute the “error on the error”, i.e. the uncertainty in F_V when we estimate it by Monte Carlo. Let us now discuss each of these in turn.

Considering first the estimator normalization F_N , one can show that it is given by the following Monte Carlo average over pairs of simulations $(b_{\ell m}, b'_{\ell m})$.

$$F_N = \left\langle \frac{1}{32} (\partial_{\ell m} Q[\tilde{b}, \tilde{b}, \tilde{b}]) (T \partial Q[s, s, s])_{\ell m} + \frac{9}{32} (\partial_{\ell m} Q[\tilde{b}, \tilde{b}, \tilde{b}']) (T \partial Q[s, s, s'])_{\ell m} - \frac{3}{32} (\partial_{\ell m} Q[\tilde{b}, \tilde{b}, \tilde{b}]) (T \partial Q[s, s', s'])_{\ell m} - \frac{3}{32} (\partial_{\ell m} Q[\tilde{b}, \tilde{b}', \tilde{b}']) (T \partial Q[s, s, s])_{\ell m} + \left(\begin{matrix} b \leftrightarrow b' \\ s \leftrightarrow s' \end{matrix} \right) \right\rangle_{b,b'} \quad (85)$$

where $(s_{\ell m}, s'_{\ell m})$ denotes the underlying CMB realizations used in simulations (b, b') . The specific choice of coefficients here was motivated in the previous section (see discussion near Eq. (83)). This expression is a “fast MC” scheme, in the sense that the fractional error in F_N is much better than $\sqrt{2/N_{\text{mc}}}$.

Next we consider the estimator variance $F_V = \text{Var}(\hat{\mathcal{E}}_0)$. Note that in the optimal pipeline from the previous section we had $F_N = F_V$, but in the pure MC pipeline where the filter need not be precisely equal to C^{-1} , one has $F_N \neq F_V$ in general. A short calculation gives the following general expression for F_V :

$$F_V = \left\langle \left(Q[\tilde{b}, \tilde{b}, \tilde{b}] - 6Q[\tilde{b}, \tilde{b}, \tilde{b}'] \right) \left(Q[\tilde{b}, \tilde{b}, \tilde{b}] - 6Q[\tilde{b}, \tilde{b}, \tilde{b}''] \right) \right\rangle - \left\langle Q[\tilde{b}, \tilde{b}, \tilde{b}] - 6Q[\tilde{b}, \tilde{b}, \tilde{b}'] \right\rangle^2 \quad (86)$$

To write this in a slightly different way, let us temporarily imagine that we have computed the quantity

$$Q_{ij} = Q[\tilde{b}_i, \tilde{b}_i, \tilde{b}_j, \tilde{b}_j] \quad (87)$$

for every pair of simulations $(\tilde{b}_i, \tilde{b}_j)$. Note that computing every Q_{ij} has computational cost $\mathcal{O}(N_{\text{mc}}^2)$, which is something we are trying to avoid, but we will address this shortly. Then the following estimator has expectation value $\langle \hat{F}_V \rangle = F_V$:

$$\begin{aligned} \hat{F}_V = & \frac{1}{N_{\text{mc}}} \sum_i Q_{ii}^2 - \frac{12}{N_2} \sum_{\{ij\}} Q_{ii} Q_{ij} + \frac{36}{N_3} \sum_{\{ijk\}} Q_{ij} Q_{ik} \\ & - \frac{1}{N_2} \sum_{\{ij\}} Q_{ii}^2 Q_{jj}^2 + \frac{12}{N_3} \sum_{\{ijk\}} Q_{ii} Q_{jk} - \frac{36}{N_4} \sum_{\{ijkl\}} Q_{ij} Q_{kl} \end{aligned} \quad (88)$$

where we have defined $N_k = N_{\text{mc}}(N_{\text{mc}} - 1) \cdots (N_{\text{mc}} - k + 1)$, and $\sum_{\{ijkl\dots\}}$ denotes a sum over *distinct* indices i, j, k, \dots between 1 and N_{mc} . This can be simplified slightly by defining

$$R_{ij} = \begin{cases} 6Q_{ij} - Q_{ii} - Q_{jj} & \text{if } i \neq j \\ 0 & \text{if } i = j \end{cases} \quad (89)$$

A short calculation then shows that \hat{F}_V simplifies to:

$$\hat{F}_V = \frac{1}{N_3} \sum_{\{ijk\}} R_{ij} R_{ik} - \frac{1}{N_4} \sum_{\{ijkl\}} R_{ij} R_{kl} \quad (90)$$

We would also like to estimate the “error on the error”, i.e. the variance of \hat{F}_V . It is easy to see that the following estimator has expectation value $\text{Var}(\hat{F}_V)$:

$$\hat{\Sigma} = (\hat{F}_V)^2 - \frac{1}{N_6} \sum_{\{ijklmn\}} R_{ij} R_{ik} R_{lm} R_{ln} + \frac{2}{N_7} \sum_{\{ijklmno\}} R_{ij} R_{ik} R_{lm} R_{no} - \frac{1}{N_8} \sum_{\{ijklmnop\}} R_{ij} R_{kl} R_{mn} R_{op} \quad (91)$$

Evaluating $\hat{\Sigma}$ in this form has $\mathcal{O}(N_{\text{mc}}^8)$ computational cost, which may be a problem in practice. In Appendix F we give an equivalent expression with lower cost.

Summarizing results in this section so far, we have expressed the unnormalized estimator $\hat{\mathcal{E}}_0$, the normalization F_N , the variance F_V , and the “error on the error” Σ as Monte Carlo averages (Eqs. (84), (85), (90), (91)). These expressions contain double Monte Carlo averages over pairs of simulations (b, b') , naively leading to $\mathcal{O}(N_{\text{mc}}^2)$ computational cost. We avoid this as follows. We divide the ensemble of N_{mc} simulations into (N_{mc}/M) subsets containing M simulations each. For each such subset, we evaluate Eqs. (84), (85), (90), (91) using only the M simulations in the subset (replacing N_{mc} when it appears by M of course). We then average over all subsets to obtain our final estimates for $\hat{\mathcal{E}}_0, F_N, F_V$, and Σ . This reduces computational cost from $\mathcal{O}(N_{\text{mc}}^2)$ to $\mathcal{O}(N_{\text{mc}}M)$.

For a fixed total number of Monte Carlo simulations N_{mc} , the larger we choose M , the more accurate our estimate for the variance F_V will be, but the computational cost of the trispectrum pipeline will also increase. Note that we must choose $M \geq 8$ in order for the expression (91) for $\hat{\Sigma}$ to make sense. We have found that $M = 16$ or $M = 32$ is usually a good compromise.

X. WMAP RESULTS AND INTERPRETATION

We conclude this paper by constraining the parameters $g_{NL}^{\text{loc}}, g_{NL}^{\sigma^4}$, and $g_{NL}^{(\partial\sigma)^4}$ from WMAP data.

In WMAP, the C^{-1} -filtering operation is computationally feasible, so we can use the optimal pipeline from §IX A. We implement C^{-1} -filtering using the multigrid conjugate gradient algorithm from Appendix A of [88]. The C^{-1} filter optimally combines data from the six V-band and W-band WMAP channels (V1,V2,W1,W2,W3,W4), and incorporates the kq75 sky mask by assigning infinite variance to masked pixels. The filter marginalizes foreground templates, sky monopoles, and dipoles in an analogous way, by assigning infinite variance to the appropriate pixel-space modes, independently in each of the six channels. These details of the filtering are the same as the optimal bispectrum analysis in the WMAP nine-year results paper [34] (see also [89]).

We ran the optimal pipeline with $N_{\text{mc}} = 2048$ Monte Carlo simulations, which turned out to be overkill: the “error on the error” due to the finite number of simulations was 0.4% for the local g_{NL} , or 0.05% for the other two trispectra. The constraints from our pipeline are:

$$\begin{aligned} g_{NL}^{\text{loc}} &= (-3.71 \pm 2.19) \times 10^5 \\ g_{NL}^{\dot{\sigma}^4} &= (-2.32 \pm 3.09) \times 10^6 \\ g_{NL}^{(\partial\sigma)^4} &= (-9.07 \pm 6.33) \times 10^5 \end{aligned} \tag{92}$$

No statistically significant deviation from Gaussian statistics is seen. This is the first constraint on the $(\partial\sigma)^4$ trispectrum. Constraints on the other two trispectra have been previously reported as follows.

The optimal estimator for g_{NL}^{loc} has also been implemented in [19], where the constraint $g_{NL}^{\text{loc}} = (-3.3 \pm 2.2) \times 10^5$ was obtained. This agrees nearly perfectly with our result in Eq. (92): the error bars are identical and the central values differ by 0.2σ . This is expected since the optimal estimator contains no free parameters. The $g_{NL}^{\dot{\sigma}^4}$ trispectrum was studied in [17], where the constraint $g_{NL}^{\dot{\sigma}^4} = (-2.88 \pm 6.94)$ was obtained.⁸ The smaller error bar in Eq. (92) is partly due to our use of WMAP9 data rather than WMAP5, and partly due to our use of the optimal estimator.

The g_{NL} central values in Eq. (92) are slightly biased by gravitational lensing. We can study the bias semianalytically using the Fisher matrix. Since the lensing trispectrum T_{lens} is not contact factorizable, we cannot use the exact Fisher matrix algorithm (§VIB), but since T_{lens} is exchange factorizable, we can still use the Monte Carlo Fisher matrix algorithm (§VIA).

Using a Fisher matrix forecast with WMAP9 noise levels, we find that the correlation coefficients of the lensing trispectrum with the local, $\dot{\sigma}^4$, and $(\partial\sigma)^4$ trispectra are 0.02, 0.15, and 0.14 respectively, and the total signal-to-noise of the CMB lensing trispectrum is only 2.1. This makes it intuitively clear that the lensing bias is small.

To quantify this better, we can estimate the lensing bias to each of the g_{NL} parameters semianalytically as follows. For any primordial trispectrum T , we approximate the bias as $\Delta g_{NL} = F(T, T_{\text{lens}})/F(T, T)$. This gives the following estimates for lensing bias:

$$\Delta g_{NL}^{\text{loc}} = 9.24 \times 10^3 \quad \Delta g_{NL}^{\dot{\sigma}^4} = 8.82 \times 10^5 \quad \Delta g_{NL}^{(\partial\sigma)^4} = 1.71 \times 10^5 \tag{93}$$

which are 0.04σ , 0.3σ , and 0.3σ shifts respectively. Subtracting lensing bias, our final “bottom line” trispectrum constraints are:

$$\begin{aligned} g_{NL}^{\text{loc}} &= (-3.80 \pm 2.19) \times 10^5 \\ g_{NL}^{\dot{\sigma}^4} &= (-3.20 \pm 3.09) \times 10^6 \\ g_{NL}^{(\partial\sigma)^4} &= (-10.8 \pm 6.33) \times 10^5 \end{aligned} \tag{94}$$

The above semianalytic prescription for lensing bias is approximate, since it is only valid to lowest order in $C_\ell^{\phi\phi}$, and also approximates the noise covariance of the survey as all-sky isotropic. Note that since the CMB lensing trispectrum is not scale-invariant, the preceding Fisher matrix based results are specific to WMAP noise levels, and lensing will be a larger effect in Planck. For WMAP, where lensing is small, the semianalytic bias correction is adequate, but for Planck a more accurate treatment will be necessary.

Each “bottom line” trispectrum constraint in Eq. (94) is a constraint on a single g_{NL} parameter assuming that the other g_{NL} -parameters are zero. We also consider the case of a joint constraint on the parameters $(g_{NL}^{\dot{\sigma}^4}, g_{NL}^{(\partial\sigma)^4})$, which are 75% correlated. It is convenient to introduce the vector notation $g_i = (g_{NL}^{\dot{\sigma}^4}, g_{NL}^{(\partial\sigma)^4})$. Let F_{ij} be the two-by-two Fisher matrix, which can be constructed as follows. The diagonal is given by $F_{ii} = 1/\sigma_i^2$, where σ_i is the

⁸ The parameter t_{NL}^{equil} defined in [17] is related to our $g_{NL}^{\dot{\sigma}^4}$ by $t_{NL}^{\text{equil}} = (27/25)g_{NL}^{\dot{\sigma}^4}$.

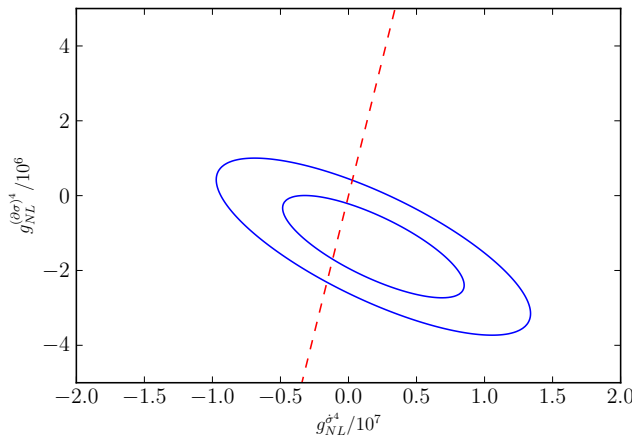


FIG. 2: 68% and 95% confidence regions in the $(g_{NL}^{\dot{\sigma}^4}, g_{NL}^{(\partial\sigma)^4})$ plane, with the Lorentz invariant model in Eq. (99) shown as the dashed line.

g_{NL} statistical error in Eq. (94). The off-diagonal is then given by $F_{12} = r_{12}F_{11}^{1/2}F_{22}^{1/2}$, where $r_{12} = 0.7558$ is the correlation coefficient from Eq. (77). From this procedure we obtain the Fisher matrix:

$$F_{ij} = \begin{pmatrix} 1.05 & 3.86 \\ 3.86 & 25.0 \end{pmatrix} \times 10^{-13} \quad (95)$$

Let $\hat{g}_i = (-3.20 \times 10^6, -1.08 \times 10^6)$ be the vector of g_{NL} estimates appearing in Eq. (94). Now for a given parameter vector g_i , we define a trispectrum χ^2 -value by:⁹

$$\chi^2(g) = ((Fg)_i - F_{ii}\hat{g}_i)F_{ij}^{-1}((Fg)_j - F_{jj}\hat{g}_j) \quad (96)$$

This χ^2 can be thresholded to obtain constraints in various parameter spaces of interest. For example, we can plot error ellipses in the $(g_{NL}^{\dot{\sigma}^4}, g_{NL}^{(\partial\sigma)^4})$ -plane, showing the off-diagonal correlation (Fig. 2). The 68% and 95% regions are obtained by thresholding at $\chi^2 = 2.279$ and $\chi^2 = 5.991$ respectively, as appropriate for a χ^2 random variable with two degrees of freedom.

We conclude with some brief physical interpretation. In single-field inflation, only the quartic operator $\dot{\pi}^4$ is allowed by the symmetries to induce a large trispectrum without generating an even larger bispectrum. Its coefficient M_4^4 in the action (9) is related to $g_{NL}^{\dot{\sigma}^4}$ by Eq. (13). Using our WMAP constraint from Eq. (94), we get the following constraint on M_4 :

$$(-2.47 \times 10^{15}) < \frac{M_4^4 c_s^3}{H^4} < (7.86 \times 10^{14}) \quad (95\% \text{ CL}) \quad (97)$$

We can develop a more intuitive understanding of this limit by noticing the following two facts [31]. First, in the case where in single field inflation this operator leads to observable non-Gaussianities, the speed of sound is not expected to be parametrically smaller than one: $c_s \lesssim 1$. Second, the unitarity bound of the theory, Λ_U , scales as $\Lambda_U^4 \sim 16\pi^2(\dot{H}M_{\text{Pl}}^2)^2 M_4^{-4}$. Therefore the limit in Eq. (97) translates to $g_{NL}^{\dot{\sigma}^4} A_\zeta \sim (H^4/\Lambda_U^4) \lesssim 10^{-3}$, which is of order the inverse square root of the number of signal-dominated modes in WMAP, as expected from a Fisher matrix analysis.

In multifield inflation, the limits above can be translated into limits on the ratios $H/(2\pi\Lambda_i)$ between the de Sitter temperature $H/(2\pi)$ during inflation and the scale suppressing the higher dimension operators in the action (12), in this way effectively mapping cosmological information into constraints of parameters of a fundamental Lagrangian.¹⁰

⁹ To derive this χ^2 , we note that the unnormalized trispectrum estimator $F_{ii}\hat{g}_i$ has expectation value $F_{ij}g_j$ and covariance matrix $\text{Cov}(F_{ii}\hat{g}_i, F_{jj}\hat{g}_j) = F_{ij}$.

¹⁰ Some readers might wonder why we call the effective field theory of inflation as a fundamental theory. Even though it is just an effective theory valid up to a scale of order Λ , this energy scale is still extremely large, and indeed quite fundamental. Furthermore, since we are not probing directly the energy scale active during inflation, but we do this only indirectly through the CMB and the LSS, the effective field theory of inflation is the only theory we are testing through observations, unless we make further assumptions.

Generally, our results show that $(H/(2\pi\Lambda))^4$ must be smaller than 10^{-2} or 10^{-3} . This tells us that the quartic interactions are still largely unconstrained, and new cosmological probes, such as Large Scale Structure surveys, will be required to significantly improve the limits. For example, if Λ_2 and Λ_3 are assumed to be zero, then our WMAP constraint on $g_{NL}^{\dot{\sigma}^4}$ in Eq. (94) gives the following constraint on Λ_1 :

$$-8.09 \times 10^{-3} < \frac{1}{(2\pi)^4} \frac{H^4}{\Lambda_1^4} < 2.57 \times 10^{-3} \quad (95\% \text{ CL}) \quad (98)$$

As another example, consider a one-parameter space consisting of the Lorentz-invariant quartic interaction:

$$S = \int d^4x \sqrt{-g} \left(\frac{1}{2} (\partial_\mu \sigma)^2 + \frac{1}{\Lambda^4} (\partial_\mu \sigma)^2 (\partial_\nu \sigma)^2 \right) \quad (99)$$

For a given value of Λ , we use Eq. (14) to compute g_{NL} coefficients, use Eq. (78) to absorb $g_{NL}^{\dot{\sigma}^2(\partial\sigma)^2}$ into the values of $g_{NL}^{\dot{\sigma}^4}$ and $g_{NL}^{(\partial\sigma)^4}$, then compute χ^2 using Eq. (96). Thresholding this χ^2 in Eq. (96) at $\Delta\chi^2 = 4$, we obtain the 95% confidence limits:

$$-4.42 \times 10^{-4} < \frac{1}{(2\pi)^4} \frac{H^4}{\Lambda^4} < 4.00 \times 10^{-5} \quad (95\% \text{ CL}) \quad (100)$$

XI. DISCUSSION

The main conclusions of this paper are as follows:

- To lowest order in the derivative expansion, the quartic operators allowed by the symmetries of inflation are $\dot{\sigma}^4$, $\dot{\sigma}^2(\partial\sigma)^2$, and $(\partial\sigma)^4$. In single-field inflation, only the $\dot{\sigma}^4$ operator is allowed by the symmetries to induce a large trispectrum without generating an even larger bispectrum, but multifield inflation allows an arbitrary linear combination of the three operators. A Fisher matrix analysis shows that there is one near-degeneracy between these three operators, which we can use to approximate the $\dot{\sigma}^2(\partial\sigma)^2$ trispectrum as a linear combination of $\dot{\sigma}^4$ and $(\partial\sigma)^4$.
- Based on this analysis, we propose the parameter space $(g_{NL}^{\text{loc}}, g_{NL}^{\dot{\sigma}^4}, g_{NL}^{(\partial\sigma)^4})$ as a starting point for analyzing inflationary 4-point signals. This is roughly analogous to the parameter space $(f_{NL}^{\text{loc}}, f_{NL}^{\text{eq}}, f_{NL}^{\text{orth}})$ for the 3-point function. It will be interesting to explore 4-point signals beyond these leading ones. In particular, “exchange” trispectra arising from cubic operators and exchange of a light field during inflation are not included in this parameter space, and would be interesting to study in future work.
- We propose two factorizability conditions for the trispectrum, contact factorizability and exchange factorizability, and study the contact factorizable case in detail. We argue that, in order to apply to operators with spatial derivatives such as $(\partial\sigma)^4$, the definition of factorizability for the trispectrum must include higher-spin fields.
- For each of our trispectra, we write the CMB trispectrum as either a single integral over a radial coordinate r (in the case of the local trispectrum) or a double integral over (τ_E, r) using a Feynman diagram (in the case of the quartic operator trispectra). By approximating the integral by a finite sum, we represent the trispectrum as a sum of a large number of factorizable terms, then apply an optimization algorithm to obtain a compact factorizable representation.
- We emphasize that the final compact representation obtained in this way approximates the exact trispectrum in a controlled sense: the two are nearly equal in the metric defined by the Fisher matrix. This is because our integration scheme includes an end-to-end Fisher matrix based convergence test (Appendix D), and the optimization algorithm is also guaranteed to converge in the Fisher matrix metric.
- We develop a toolkit of algorithms which can be applied to factorizable trispectra, including estimator evaluation, non-Gaussian simulation (Appendix B), and Fisher matrix calculation.
- We develop an optimal trispectrum pipeline and apply it to WMAP, finding consistency with Gaussian statistics. We also develop a “pure MC” pipeline which scales to Planck. The optimal pipeline can be used if C^{-1} is computationally affordable and lensing bias is small enough to be estimated semianalytically. The pure MC pipeline relaxes both of these assumptions but is slower to converge.

- The tools we have developed in this paper are sufficient to analyze the local, δ^4 , $\delta^2(\partial\sigma)^2$, and $(\partial\sigma)^4$ trispectra in WMAP and Planck. However there are a few directions in which our machinery might be improved. In order to analyze exchange trispectra, one would need to generalize the optimization algorithm from §VII. It would be interesting to improve the sensitivity of our pipeline to noise modeling, as suggested in §III D. Finally, in cases where C^{-1} is affordable, we currently have to choose between the fast convergence of the optimal pipeline (§IX A) and precise calculation of lensing bias in the pure MC pipeline (§IX B).

Acknowledgements

Research at Perimeter Institute is supported by the Government of Canada through Industry Canada and by the Province of Ontario through the Ministry of Research & Innovation. Some computations were performed on the GPC cluster at the Scinet HPC Consortium. SciNet is funded by the Canada Foundation for Innovation under the auspices of Compute Canada, the Government of Ontario, and the University of Toronto. KMS was supported by an NSERC Discovery Grant. LS is supported by DOE Early Career Award DE-FG02-12ER41854 and the National Science Foundation under PHY-1068380. MZ is supported in part by the NSF grants AST-0907969, PHY-1213563 and AST-1409709.

-
- [1] D. H. Lyth, C. Ungarelli, and D. Wands, *Phys.Rev.* **D67**, 023503 (2003), astro-ph/0208055.
[2] M. Zaldarriaga, *Phys.Rev.* **D69**, 043508 (2004), astro-ph/0306006.
[3] E. Komatsu, D. N. Spergel, and B. D. Wandelt, *Astrophys.J.* **634**, 14 (2005), astro-ph/0305189.
[4] L. Senatore and M. Zaldarriaga, *JHEP* **1204**, 024 (2012), 1009.2093.
[5] P. Creminelli, A. Nicolis, L. Senatore, M. Tegmark, and M. Zaldarriaga, *JCAP* **0605**, 004 (2006), astro-ph/0509029.
[6] L. Senatore, K. M. Smith, and M. Zaldarriaga, *JCAP* **1001**, 028 (2010), 0905.3746.
[7] S. R. Behbahani, M. Mirbabayi, L. Senatore, and K. M. Smith, (2014), 1407.7042.
[8] J. Fergusson, M. Liguori, and E. Shellard, *Phys.Rev.* **D82**, 023502 (2010), 0912.5516.
[9] Planck Collaboration, P. Ade *et al.*, (2013), 1303.5084.
[10] J. J. M. Carrasco, M. P. Hertzberg, and L. Senatore, *JHEP* **1209**, 082 (2012), 1206.2926.
[11] D. Babich, P. Creminelli, and M. Zaldarriaga, *JCAP* **0408**, 009 (2004), astro-ph/0405356.
[12] J. M. Maldacena, *JHEP* **0305**, 013 (2003), astro-ph/0210603.
[13] L. Senatore and M. Zaldarriaga, *JCAP* **1208**, 001 (2012), 1203.6884.
[14] T. Baldauf, U. Seljak, L. Senatore, and M. Zaldarriaga, *JCAP* **1110**, 031 (2011), 1106.5507.
[15] P. Vielva and J. Sanz, *Mon.Not.Roy.Astron.Soc.* **404**, 895 (2010), 0910.3196.
[16] J. Smidt *et al.*, *Phys.Rev.* **D81**, 123007 (2010), 1004.1409.
[17] J. Fergusson, D. Regan, and E. Shellard, (2010), 1012.6039.
[18] C. Hikage and T. Matsubara, *Mon.Not.Roy.Astron.Soc.* **425**, 2187 (2012), 1207.1183.
[19] T. Sekiguchi and N. Sugiyama, *JCAP* **1309**, 002 (2013), 1303.4626.
[20] L.-M. Wang and M. Kamionkowski, *Phys.Rev.* **D61**, 063504 (2000), astro-ph/9907431.
[21] K. M. Smith and M. Zaldarriaga, *Mon.Not.Roy.Astron.Soc.* **417**, 2 (2011), astro-ph/0612571.
[22] M. Bucher, B. Van Tent, and C. S. Carvalho, *Mon.Not.Roy.Astron.Soc.* **407**, 2193 (2010), 0911.1642.
[23] S. Donzelli, F. K. Hansen, M. Liguori, D. Marinucci, and S. Matarrese, *Astrophys.J.* **755**, 19 (2012), 1202.1478.
[24] J. Byun and R. Bean, *JCAP* **1309**, 026 (2013), 1303.3050.
[25] S. Das *et al.*, *Phys.Rev.Lett.* **107**, 021301 (2011), 1103.2124.
[26] S. Das *et al.*, *JCAP* **1404**, 014 (2014), 1301.1037.
[27] A. van Engelen *et al.*, *Astrophys.J.* **756**, 142 (2012), 1202.0546.
[28] K. Story *et al.*, (2014), 1412.4760.
[29] Planck Collaboration, P. Ade *et al.*, *Astron.Astrophys.* **571**, A17 (2014), 1303.5077.
[30] C. Cheung, P. Creminelli, A. L. Fitzpatrick, J. Kaplan, and L. Senatore, *JHEP* **0803**, 014 (2008), 0709.0293.
[31] L. Senatore and M. Zaldarriaga, *JCAP* **1101**, 003 (2011), 1004.1201.
[32] X. Chen, B. Hu, M.-x. Huang, G. Shiu, and Y. Wang, *JCAP* **0908**, 008 (2009), 0905.3494.
[33] F. Arroja, S. Mizuno, K. Koyama, and T. Tanaka, *Phys.Rev.* **D80**, 043527 (2009), 0905.3641.
[34] WMAP, C. Bennett *et al.*, *Astrophys.J.Suppl.* **208**, 20 (2013), 1212.5225.
[35] N. Bartolo, M. Fasiello, S. Matarrese, and A. Riotto, *JCAP* **1009**, 035 (2010), 1006.5411.
[36] P. Creminelli, G. D’Amico, M. Musso, J. Norena, and E. Trincherini, *JCAP* **1102**, 006 (2011), 1011.3004.
[37] N. Bartolo, E. Dimastrogiovanni, and M. Fasiello, *JCAP* **1309**, 037 (2013), 1305.0812.
[38] F. Arroja, N. Bartolo, E. Dimastrogiovanni, and M. Fasiello, *JCAP* **1311**, 005 (2013), 1307.5371.
[39] M. Sasaki and E. D. Stewart, *Prog.Theor.Phys.* **95**, 71 (1996), astro-ph/9507001.
[40] A. A. Starobinsky, *JETP Lett.* **42**, 152 (1985).
[41] M. Sasaki and T. Tanaka, *Prog.Theor.Phys.* **99**, 763 (1998), gr-qc/9801017.

- [42] H.-C. Lee, M. Sasaki, E. D. Stewart, T. Tanaka, and S. Yokoyama, *JCAP* **0510**, 004 (2005), astro-ph/0506262.
- [43] X. Chen and Y. Wang, *Phys.Rev.* **D81**, 063511 (2010), 0909.0496.
- [44] X. Chen and Y. Wang, *JCAP* **1004**, 027 (2010), 0911.3380.
- [45] P. Creminelli, *Phys.Rev.* **D85**, 041302 (2012), 1108.0874.
- [46] J. M. Maldacena and G. L. Pimentel, *JHEP* **1109**, 045 (2011), 1104.2846.
- [47] F. Bernardeau and J.-P. Uzan, *Phys.Rev.* **D66**, 103506 (2002), hep-ph/0207295.
- [48] F. Bernardeau and J.-P. Uzan, *Phys.Rev.* **D67**, 121301 (2003), astro-ph/0209330.
- [49] D. Seery, J. E. Lidsey, and M. S. Sloth, *JCAP* **0701**, 027 (2007), astro-ph/0610210.
- [50] X. Chen, M.-x. Huang, and G. Shiu, *Phys.Rev.* **D74**, 121301 (2006), hep-th/0610235.
- [51] D. Seery and J. E. Lidsey, *JCAP* **0701**, 008 (2007), astro-ph/0611034.
- [52] C. T. Byrnes, M. Sasaki, and D. Wands, *Phys.Rev.* **D74**, 123519 (2006), astro-ph/0611075.
- [53] F. Bernardeau and T. Brunier, *Phys.Rev.* **D76**, 043526 (2007), 0705.2501.
- [54] F. Arroja and K. Koyama, *Phys.Rev.* **D77**, 083517 (2008), 0802.1167.
- [55] D. Seery, M. S. Sloth, and F. Vernizzi, *JCAP* **0903**, 018 (2009), 0811.3934.
- [56] K. T. Engel, K. S. Lee, and M. B. Wise, *Phys.Rev.* **D79**, 103530 (2009), 0811.3964.
- [57] Q.-G. Huang, *JCAP* **0905**, 005 (2009), 0903.1542.
- [58] X. Gao and B. Hu, *JCAP* **0908**, 012 (2009), 0903.1920.
- [59] E. Kawakami, M. Kawasaki, K. Nakayama, and F. Takahashi, *JCAP* **0909**, 002 (2009), 0905.1552.
- [60] S. Mizuno, F. Arroja, and K. Koyama, *Phys.Rev.* **D80**, 083517 (2009), 0907.2439.
- [61] N. Bartolo, E. Dimastrogiovanni, S. Matarrese, and A. Riotto, *JCAP* **0911**, 028 (2009), 0909.5621.
- [62] C. A. Valenzuela-Toledo and Y. Rodriguez, *Phys.Lett.* **B685**, 120 (2010), 0910.4208.
- [63] Q.-G. Huang, *JCAP* **1007**, 025 (2010), 1004.0808.
- [64] K. Izumi and S. Mukohyama, *JCAP* **1006**, 016 (2010), 1004.1776.
- [65] X. Gao and C. Lin, *JCAP* **1011**, 035 (2010), 1009.1311.
- [66] L. Leblond and E. Pajer, *JCAP* **1101**, 035 (2011), 1010.4565.
- [67] D. Langlois and T. Takahashi, *JCAP* **1102**, 020 (2011), 1012.4885.
- [68] J. Meyers and N. Sivanandam, *Phys.Rev.* **D84**, 063522 (2011), 1104.5238.
- [69] I. Agullo, J. Navarro-Salas, and L. Parker, *JCAP* **1205**, 019 (2012), 1112.1581.
- [70] J. Elliston, L. Alabidi, I. Huston, D. Mulryne, and R. Tavakol, *JCAP* **1209**, 001 (2012), 1203.6844.
- [71] G. J. Anderson, D. J. Mulryne, and D. Seery, *JCAP* **1210**, 019 (2012), 1205.0024.
- [72] S. Renaux-Petel, *JCAP* **1307**, 005 (2013), 1302.6978.
- [73] A. A. Abolhasani, R. Emami, J. T. Firouzjaee, and H. Firouzjahi, *JCAP* **1308**, 016 (2013), 1302.6986.
- [74] S. Renaux-Petel, *JCAP* **1308**, 017 (2013), 1303.2618.
- [75] G. Leung, E. R. Tarrant, C. T. Byrnes, and E. J. Copeland, *JCAP* **1308**, 006 (2013), 1303.4678.
- [76] M. Fasiello, *JCAP* **1312**, 033 (2013), 1303.5015.
- [77] C. T. Byrnes, S. Nurmi, G. Tasinato, and D. Wands, *Europhys.Lett.* **103**, 19001 (2013), 1306.2370.
- [78] W. Hu, *Phys. Rev.* **D64**, 083005 (2001), astro-ph/0105117.
- [79] D. M. Regan and E. P. S. Shellard, *Phys. Rev.* **D82**, 023520 (2010), 1004.2915.
- [80] B. D. Sherwin and S. Das, (2010), 1011.4510.
- [81] S. Plaszczyński, A. Lavabre, L. Perotto, and J.-L. Starck, *Astron.Astrophys.* **544**, A27 (2012), 1201.5779.
- [82] T. Namikawa, D. Hanson, and R. Takahashi, *Mon.Not.Roy.Astron.Soc.* **431**, 609 (2013), 1209.0091.
- [83] A. Lewis, A. Challinor, and A. Lasenby, *Astrophys.J.* **538**, 473 (2000), astro-ph/9911177.
- [84] D. Baumann and D. Green, *Phys.Rev.* **D85**, 103520 (2012), 1109.0292.
- [85] D. Green, M. Lewandowski, L. Senatore, E. Silverstein, and M. Zaldarriaga, *JHEP* **1310**, 171 (2013), 1301.2630.
- [86] D. Munshi *et al.*, *Mon.Not.Roy.Astron.Soc.* **412**, 1993 (2011), 0910.3693.
- [87] ACT Collaboration, A. van Engelen *et al.*, (2014), 1412.0626.
- [88] K. M. Smith, O. Zahn, and O. Doré, *Phys. Rev.* **D76**, 043510 (2007), 0705.3980.
- [89] K. M. Smith, L. Senatore, and M. Zaldarriaga, *JCAP* **0909**, 006 (2009), 0901.2572.
- [90] K. M. Smith, W. Hu, and M. Kaplinghat, *Phys.Rev.* **D70**, 043002 (2004), astro-ph/0402442.
- [91] C. Li, T. L. Smith, and A. Cooray, *Phys.Rev.* **D75**, 083501 (2007), astro-ph/0607494.
- [92] M. Liguori, S. Matarrese, and L. Moscardini, *Astrophys. J.* **597**, 57 (2003), astro-ph/0306248.
- [93] D. Hanson, K. M. Smith, A. Challinor, and M. Liguori, *Phys.Rev.* **D80**, 083004 (2009), 0905.4732.
- [94] A. Lewis, *Phys. Rev.* **D71**, 083008 (2005), astro-ph/0502469.
- [95] WMAP, G. Hinshaw *et al.*, *Astrophys.J.Suppl.* **208**, 19 (2013), 1212.5226.
- [96] P. Creminelli, L. Senatore, M. Zaldarriaga, and M. Tegmark, *JCAP* **0703**, 005 (2007), astro-ph/0610600.
- [97] U. Seljak and M. Zaldarriaga, *Astrophys.J.* **469**, 437 (1996), astro-ph/9603033.
- [98] A. Barnett, D. Feng, J. Steed, and L. Goldfarb, *Computer Physics Communications* **8**, 377 (1974).
- [99] D. Hanson, A. Challinor, G. Efstathiou, and P. Bielewicz, *Phys.Rev.* **D83**, 043005 (2011), 1008.4403.

Appendix A: Wigner d -functions and spin- s spherical harmonics

In this appendix, we briefly review properties of the Wigner d -function $d_{ss'}^\ell(\theta)$ and spin- s spherical harmonics (${}_s Y_{\ell m}$) which will be used in the text.

For integers s, s' , the Wigner d -function $d_{ss'}^\ell(\theta)$ is defined for $\ell \geq \max(|s|, |s'|)$ and satisfies the orthogonality condition:

$$\int_{-1}^1 d(\cos \theta) d_{ss'}^{\ell_1}(\theta) d_{ss'}^{\ell_2}(\theta) = \frac{2}{2\ell + 1} \delta_{\ell_1 \ell_2} \quad (\text{A1})$$

as well as the identity:

$$d_{-s, -s'}^\ell(\theta) = d_{s', s}^\ell(\theta) = (-1)^{s+s'} d_{ss'}^\ell(\theta) \quad (\text{A2})$$

The Wigner d -functions can be computed using the recursion relation

$$\alpha_{ss'}^{\ell+1}(\theta) d_{ss'}^{\ell+1}(\theta) - (2\ell + 1) \left(\cos \theta - \frac{ss'}{\ell(\ell + 1)} \right) d_{ss'}^\ell(\theta) + \alpha_{ss'}^\ell(\theta) d_{ss'}^{\ell-1}(\theta) = 0 \quad (\ell \geq \max(|s|, |s'|)) \quad (\text{A3})$$

where $\alpha_{ss'}^\ell = \sqrt{(\ell^2 - s^2)(\ell^2 - (s')^2)}/\ell$. If $s' \geq |s|$, then initial conditions for the recursion are given by:

$$d_{ss'}^{s'}(\theta) = \sqrt{\frac{(2s')!}{(s' - |s|)!(s' + |s|)!}} \left(\frac{1 + \cos \theta}{2} \right)^{(s'+s)/2} \left(\frac{1 - \cos \theta}{2} \right)^{(s'-s)/2} \quad (s' \geq |s|) \quad (\text{A4})$$

Initial conditions for arbitrary (s, s') can be obtained through use of Eq. (A2).

A spin- s field (${}_s f$) is a field whose value at a point $\hat{\mathbf{n}}$ depends on a choice $\{\hat{e}_1, \hat{e}_2\}$ of local orthonormal frame at $\hat{\mathbf{n}}$, such that under a change of frame $(\hat{e}_1 \pm i\hat{e}_2) \rightarrow e^{\pm i\alpha}(\hat{e}_1 \pm i\hat{e}_2)$, the field value transforms as $({}_s f) \rightarrow e^{-is\alpha}({}_s f)$.

The spin-raising operator $\bar{\partial}$ and spin-lowering operator ∂ are defined by:

$$\partial = m_a \nabla^a \quad \bar{\partial} = m_a^* \nabla^a \quad (\text{A5})$$

where we have defined the spin-1 vector field $m_a = (\hat{e}_1 - i\hat{e}_2)$. The spin-raising and spin-lowering operators transform a spin- s field to fields of spin $(s + 1)$ and $(s - 1)$ respectively.

The spin- s spherical harmonics (${}_s Y_{\ell m}$) are an orthonormal basis for spin- s fields on the full sky, defined for $\ell \geq |s|$ and $-\ell \leq m \leq \ell$. The spin-raising and spin-lowering operators act on the $({}_s Y_{\ell m})$ by:

$$\partial({}_s Y_{\ell m}) = \sqrt{(\ell - s)(\ell + s + 1)}({}_{s+1} Y_{\ell m}) \quad \bar{\partial}({}_s Y_{\ell m}) = -\sqrt{(\ell + s)(\ell - s + 1)}({}_{s-1} Y_{\ell m}) \quad (\text{A6})$$

The spin- s harmonics satisfy the identity:

$$({}_s Y_{\ell m})^* = (-1)^{s+m} ({}_{-s} Y_{\ell, -m}) \quad (\text{A7})$$

and are related to Wigner d -functions by the following sum rule:

$$\sum_{m=-\ell}^{\ell} ({}_s Y_{\ell m}(\hat{\mathbf{n}})) ({}_{s'} Y_{\ell m}(\hat{\mathbf{n}}'))^* = (-1)^s \frac{2\ell + 1}{4\pi} d_{ss'}^\ell(\theta) \quad (\text{A8})$$

where $\theta = \cos^{-1}(\hat{\mathbf{n}} \cdot \hat{\mathbf{n}}')$ is the angle between unit vectors $\hat{\mathbf{n}}, \hat{\mathbf{n}}'$. The sum rule applies in the ‘‘two-point’’ frame where the local frame vectors \hat{e}_1, \hat{e}'_1 at points $\hat{\mathbf{n}}, \hat{\mathbf{n}}'$ have been chosen to point along the geodesic connecting the two points. (Note that the LHS of the sum rule depends on the choice of frames, but the RHS does not, so it must be understood that the sum rule applies only in the two-point frame.)

Appendix B: Non-Gaussian simulations

In [21], an algorithm was proposed for simulating a random, weakly non-Gaussian CMB realization with prescribed power spectrum and bispectrum. It is straightforward to generalize this algorithm to simulate a CMB realization with prescribed power spectrum C_ℓ and trispectrum $T_{m_1 m_2 m_3 m_4}^{\ell_1 \ell_2 \ell_3 \ell_4}$.

First, a definition. For any angular trispectrum T , define the symmetric matrix $\tilde{T}_{\ell\ell'}$ by:

$$\tilde{T}_{\ell\ell'} = \sum_{mm'} (-1)^{m+m'} T_{m(-m)m'(-m')}^{\ell\ell'\ell'}. \quad (\text{B1})$$

This matrix arises in several contexts. First, if $a_{\ell m}, b_{\ell m}$ are all-sky Gaussian random fields, then $\tilde{T}_{\ell\ell'}$ appears in the following expectation values:

$$\langle Q_T[a] \rangle = \frac{1}{8} \sum_{\ell\ell'} \tilde{T}_{\ell\ell'} C_\ell^{aa} C_{\ell'}^{aa} \quad (\text{B2})$$

$$\langle b_{\ell'm'}^* \partial_{\ell m} Q_T[a] \rangle = \left(\frac{C_\ell^{ab}}{2(2\ell+1)} \sum_{\ell'} \tilde{T}_{\ell\ell'} C_{\ell'}^{aa} \right) \delta_{\ell\ell'} \delta_{mm'} \quad (\text{B3})$$

Second, if the CMB is non-Gaussian, then the estimated CMB power spectrum $\hat{C}_\ell = (2\ell+1)^{-1} \sum_m a_{\ell m}^* a_{\ell m}$ contains a term proportional to $\tilde{T}_{\ell\ell'}$:

$$\text{Cov}(\hat{C}_\ell, \hat{C}_{\ell'}) = \frac{2C_\ell^2}{2\ell+1} \delta_{\ell\ell'} + \frac{\tilde{T}_{\ell\ell'}}{(2\ell+1)(2\ell'+1)} \quad (\text{B4})$$

Note that non-Gaussian power spectrum covariance due to the gravitational lensing trispectrum has been studied extensively (e.g. [90, 91]); Eq. (B4) generalizes to an arbitrary trispectrum.

Our non-Gaussian simulation algorithm is as follows. We first simulate a *Gaussian* field $a_{\ell m}^G$ with power spectrum C_ℓ , and then define the non-Gaussian field $a_{\ell m}^{NG}$ by:

$$a_{\ell m}^{NG} = a_{\ell m}^G + \frac{1}{4} \partial_{\ell m} Q[a_{\ell m}^G/C_\ell] - \frac{1}{8} \sum_{\ell'} \frac{\tilde{T}_{\ell\ell'}}{(2\ell+1)C_\ell C_{\ell'}} a_{\ell m}^G \quad (\text{B5})$$

A short calculation shows that the power spectrum and four-point function of the simulated field are given by:

$$\langle a_{\ell m}^{NG*} a_{\ell m}^{NG} \rangle = C_\ell + \mathcal{O}(T^2) \quad \langle a_{\ell_1 m_1}^{NG} a_{\ell_2 m_2}^{NG} a_{\ell_3 m_3}^{NG} a_{\ell_4 m_4}^{NG} \rangle_c = T_{m_1 m_2 m_3 m_4}^{\ell_1 \ell_2 \ell_3 \ell_4} + \mathcal{O}(T^2) \quad (\text{B6})$$

where $\mathcal{O}(T^2)$ denotes contributions which are second-order in the trispectrum $T_{m_1 m_2 m_3 m_4}^{\ell_1 \ell_2 \ell_3 \ell_4}$. The last term in Eq. (B5) has been included in order to avoid an order- $\mathcal{O}(T)$ correction to the power spectrum. (We note that odd $(2N+1)$ -point correlation functions of $a_{\ell m}^{NG}$ are zero, and even $(2N)$ -point connected correlation functions are of order $\mathcal{O}(T^{N-1})$.)

To apply the simulation algorithm, we need to compute $\tilde{T}_{\ell\ell'}$. In the case where T is contact factorizable we can do this using a method similar to the exact Fisher matrix algorithm from §VI B. We write $Q_T[a]$ in the abbreviated form:

$$Q_T[a] = \frac{1}{48} \sum_{I=1}^{N_{\text{fact}}} \int d^2 \hat{\mathbf{n}} M_{\alpha_I}^{A_I}(\hat{\mathbf{n}}) M_{\beta_I}^{B_I}(\hat{\mathbf{n}}) M_{\gamma_I}^{C_I}(\hat{\mathbf{n}}) M_{\delta_I}^{D_I}(\hat{\mathbf{n}}) + \text{c.c.} \quad (\text{B7})$$

where we have defined $M_s^X(\hat{\mathbf{n}}) = \sum_{\ell m} X_\ell a_{\ell m}(s Y_{\ell m}(\hat{\mathbf{n}}))$. We can compute the expectation value $\langle Q_T[a] \rangle$ using Wick's theorem and the contraction

$$\overline{M_s^X(\hat{\mathbf{n}}) M_{s'}^{X'}(\hat{\mathbf{n}})} = (-1)^s \sum_{\ell} \frac{2\ell+1}{4\pi} X_\ell X'_\ell C_\ell^{aa} \delta_{s,-s'} \quad (\text{B8})$$

obtaining:

$$\begin{aligned} \langle Q_T[a] \rangle &= \frac{1}{48} \sum_{I=1}^{N_{\text{fact}}} \sum_{\ell\ell'} \frac{(2\ell+1)(2\ell'+1)}{4\pi} C_\ell^{aa} C_{\ell'}^{aa} \left[(-1)^{\alpha_I+\gamma_I} A_\ell^I B_\ell^I C_{\ell'}^I D_{\ell'}^I \delta_{\alpha_I, -\beta_I} \delta_{\gamma_I, -\delta_I} \right. \\ &\quad \left. + (-1)^{\alpha_I+\beta_I} A_\ell^I B_{\ell'}^I C_\ell^I D_{\ell'}^I \delta_{\alpha_I, -\gamma_I} \delta_{\beta_I, -\delta_I} + (-1)^{\alpha_I+\beta_I} A_\ell^I B_{\ell'}^I C_\ell^I D_{\ell'}^I \delta_{\alpha_I, -\delta_I} \delta_{\beta_I, -\gamma_I} \right] + \text{c.c.} \quad (\text{B9}) \end{aligned}$$

Comparing with Eq. (B2) we can read off an expression for $\tilde{T}_{\ell\ell'}$ (note that we symmetrize in ℓ, ℓ'):

$$\begin{aligned} \tilde{T}_{\ell\ell'} &= \frac{(2\ell+1)(2\ell'+1)}{48\pi} \sum_{I=1}^{N_{\text{fact}}} \left[(-1)^{\alpha_I+\gamma_I} A_\ell^I B_\ell^I C_{\ell'}^I D_{\ell'}^I \delta_{\alpha_I, -\beta_I} \delta_{\gamma_I, -\delta_I} + (-1)^{\alpha_I+\beta_I} A_\ell^I B_{\ell'}^I C_\ell^I D_{\ell'}^I \delta_{\alpha_I, -\gamma_I} \delta_{\beta_I, -\delta_I} \right. \\ &\quad \left. + (-1)^{\alpha_I+\beta_I} A_\ell^I B_{\ell'}^I C_{\ell'}^I D_\ell^I \delta_{\alpha_I, -\delta_I} \delta_{\beta_I, -\gamma_I} \right] + (\ell \leftrightarrow \ell') + \text{c.c.} \quad (\text{B10}) \end{aligned}$$

This algorithm for computing $\tilde{T}_{\ell\ell'}$ can be generalized to the exchange factorizable case, using the same strategy of computing $\langle Q_T[a] \rangle$ with Wick's theorem, but we omit the details. Note that the matrix $\tilde{T}_{\ell\ell'}$ may be useful outside the context of non-Gaussian simulations, since it appears in the non-Gaussian power spectrum covariance (B4).

This generic simulation algorithm formally generates a non-Gaussian field whose power spectrum C_ℓ and trispectrum T are prescribed, up to contributions of order $\mathcal{O}(T^2)$. A significant caveat is that for some trispectrum shapes, these $\mathcal{O}(T^2)$ contributions can be large even for modest levels of non-Gaussianity. We have not experimented much with the simulation algorithm, but based on experience with the analogous bispectrum algorithm, we expect it will work well for shapes which do not have large squeezed limits, for example the $\dot{\sigma}^4$, $\dot{\sigma}^2(\partial\sigma)^2$, and $(\partial\sigma)^4$ shapes.

The local trispectra g_{NL}^{loc} and τ_{NL} have large squeezed limits, so we do not expect our generic simulation algorithm to work well in these cases. One alternate approach is to simulate 3D fields at the end of inflation, apply the relevant local operation (either $\zeta = \zeta_G + (9/25)g_{NL}^{\text{loc}}\zeta_G^3$ or $\zeta = \zeta_G + \tau_{NL}^{1/2}\zeta_G\sigma$), and then apply the CMB transfer function to generate $a_{\ell m}$'s [92]. Another approach is to reweight terms in the generic algorithm to avoid infrared divergences in specific cases (see discussion in the appendix of [93]).

The gravitational lensing trispectrum (63) is another example of a shape with a large squeezed limit, where we do not expect our generic simulation algorithm to work well. In this case the best approach is to simply simulate the lensing deflection $T(\hat{\mathbf{n}}) \rightarrow T(\hat{\mathbf{n}} + \nabla\phi(\hat{\mathbf{n}}))$ directly [94].

Appendix C: Factorizable representations for g_{NL}^{loc} , $g_{NL}^{\dot{\sigma}^4}$, $g_{NL}^{(\partial\sigma)^4}$

In §V C, we calculated the factorizable representation explicitly for the trispectrum generated by the quartic operator $\dot{\sigma}^2(\partial\sigma)^2$. In this appendix, we do the same for the g_{NL}^{loc} trispectrum, and the trispectra generated by the operators $\dot{\sigma}^4$ and $(\partial\sigma)^4$.

1. g_{NL}^{loc} shape

First we consider the g_{NL}^{loc} shape. The ζ -trispectrum was given previously in Eq. (2):

$$\langle \zeta_{\mathbf{k}_1} \zeta_{\mathbf{k}_2} \zeta_{\mathbf{k}_3} \zeta_{\mathbf{k}_4} \rangle_c = \left(\frac{54}{25} g_{NL}^{\text{loc}} P_\zeta(k_2) P_\zeta(k_3) P_\zeta(k_4) + 3 \text{ perm.} \right) (2\pi)^3 \delta^3 \left(\sum \mathbf{k}_i \right) \quad (\text{C1})$$

Following the previous calculation in §V C, we plug into the projection formula (37), replace the delta function $\delta^3(\sum \mathbf{k}_i)$ by $\int d^3 \mathbf{r} \exp(i \sum \mathbf{k}_i \cdot \mathbf{r})$, and do the angular parts of the \mathbf{k} integrals, obtaining:

$$\begin{aligned} Q_T[a] &= \frac{9}{25} g_{NL}^{\text{loc}} \int_0^\infty r^2 dr \int d^2 \hat{\mathbf{n}} \left(\prod_{i=1}^4 \int \frac{2k_i^2 dk_i}{\pi} \sum_{\ell_i m_i} j_{\ell_i}(k_i r) \Delta_{\ell_i}(k_i) a_{\ell_i m_i} Y_{\ell_i m_i}(\hat{\mathbf{n}}) \right) P_\zeta(k_2) P_\zeta(k_3) P_\zeta(k_4) \\ &= g_{NL}^{\text{loc}} \int r^2 dr \int d^2 \hat{\mathbf{n}} \left(\sum_{\ell m} \alpha_\ell(r) a_{\ell m} Y_{\ell m}(\hat{\mathbf{n}}) \right) \left(\sum_{\ell' m'} \beta_{\ell'}(r) a_{\ell' m'} Y_{\ell' m'}(\hat{\mathbf{n}}) \right)^3 \end{aligned} \quad (\text{C2})$$

where the functions $\alpha_\ell(r), \beta_\ell(r)$ were defined previously in Eq. (61). Comparing with the definition (51), we see that after replacing the r integral by a finite sum, the trispectrum is contact factorizable with all spins equal to zero.

2. $g_{NL}^{\dot{\sigma}^4}$ shape

Next we consider the quartic operator $\dot{\sigma}^4$. The ζ -trispectrum was given previously in Eq. (5):

$$\langle \zeta_{\mathbf{k}_1} \zeta_{\mathbf{k}_2} \zeta_{\mathbf{k}_3} \zeta_{\mathbf{k}_4} \rangle_c = \frac{9216}{25} A_\zeta^3 g_{NL}^{\dot{\sigma}^4} \int_{-\infty}^0 d\tau_E \tau_E^4 \left(\prod_{i=1}^4 \frac{e^{k_i \tau_E}}{k_i} \right) (2\pi)^3 \delta^3 \left(\sum \mathbf{k}_i \right) \quad (\text{C3})$$

Using the same method of calculation as in §V C, we find the following expression for $Q_T[a]$:

$$Q_T[a] = \frac{384}{25} A_\zeta^3 g_{NL}^{\dot{\sigma}^4} \int_{-\infty}^0 d\tau_E \int_0^\infty dr \tau_E^4 r^2 \int d^2 \hat{\mathbf{n}} \left(\prod_{i=1}^4 \sum_{\ell_i m_i} \int \frac{2k_i^2 dk_i}{\pi} j_{\ell_i}(k_i r) \Delta_{\ell_i}(k_i) \frac{e^{k_i \tau_E}}{k_i} a_{\ell_i m_i} Y_{\ell_i m_i}(\hat{\mathbf{n}}) \right) \quad (\text{C4})$$

Using the notation $\mu_\ell(\tau_E, r)$ defined previously in Eq. (57), we rewrite this as:

$$Q_T[a] = \frac{128}{3} g_{NL}^{\partial^4} \int_{-\infty}^0 d\tau_E \int_0^\infty dr \tau_E^4 r^2 \int d^2 \hat{\mathbf{n}} \left(\sum_{\ell m} \mu_\ell(\tau_E, r) a_{\ell m} Y_{\ell m}(\hat{\mathbf{n}}) \right)^4 \quad (\text{C5})$$

After replacing the (τ_E, r) double integral by a finite sum, $Q_T[a]$ is of contact factorizable form (50).

3. $g_{NL}^{(\partial\sigma)^4}$ shape

Finally we consider the case of a quartic operator $(\partial_i \sigma)^2 (\partial_j \sigma)^2$. The ζ -trispectrum was given previously in Eq. (7):

$$\langle \zeta_{\mathbf{k}_1} \zeta_{\mathbf{k}_2} \zeta_{\mathbf{k}_3} \zeta_{\mathbf{k}_4} \rangle_c = \frac{82944}{2575} g_{NL}^{(\partial\sigma)^4} A_\zeta^3 \int_{-\infty}^0 d\tau_E \left(\prod_{i=1}^4 \frac{(1 - k_i \tau_E) e^{k_i \tau_E}}{k_i^3} \right) \left((\mathbf{k}_1 \cdot \mathbf{k}_2)(\mathbf{k}_3 \cdot \mathbf{k}_4) + 2 \text{ perm.} \right) (2\pi)^3 \delta^3 \left(\sum \mathbf{k}_i \right) \quad (\text{C6})$$

In this case we find the following expression for $Q_T[a]$:

$$Q_T[a] = \frac{1152}{103} g_{NL}^{(\partial\sigma)^4} \int_{-\infty}^0 d\tau_E \int d^3 \mathbf{r} \frac{\partial F(\tau_E, \mathbf{r})}{\partial \mathbf{r}_i} \frac{\partial F(\tau_E, \mathbf{r})}{\partial \mathbf{r}_i} \frac{\partial F(\tau_E, \mathbf{r})}{\partial \mathbf{r}_j} \frac{\partial F(\tau_E, \mathbf{r})}{\partial \mathbf{r}_j} \quad (\text{C7})$$

where we have defined

$$F(\tau_E, \mathbf{r}) = \left(\frac{3}{5} \right)^{1/2} A_\zeta^{3/4} \int \frac{2k^2 dk}{\pi} \sum_{\ell m} \frac{(1 - k\tau_E) e^{k\tau_E}}{k^3} j_\ell(kr) \Delta_\ell(k) a_{\ell m} Y_{\ell m}(\mathbf{r}) \quad (\text{C8})$$

As in §VC we can split the gradients into radial and tangential terms using the identity:

$$\sum_i \frac{\partial F(\mathbf{r})}{\partial \mathbf{r}_i} \frac{\partial F(\mathbf{r})}{\partial \mathbf{r}_i} = \left(\frac{\partial F(\mathbf{r})}{\partial r} \right)^2 + \frac{1}{r^2} (\not\partial F)^* (\not\partial F) \quad (\text{C9})$$

where the real and tangential derivatives can be written in terms of the functions ν, ω introduced previously in Eq. (57):

$$\frac{\partial F(\tau_E, \mathbf{r})}{\partial r} = \sum_{\ell m} \nu_\ell(\tau_E, r) a_{\ell m} Y_{\ell m}(\hat{\mathbf{r}}) \quad \not\partial F(\tau_E, \mathbf{r}) = r \sum_{\ell m} \omega_\ell(\tau_E, r) a_{\ell m} ({}_1 Y_{\ell m}(\hat{\mathbf{r}})) \quad (\text{C10})$$

Plugging this in we get the representation of $Q_T[a]$ in contact factorizable form:

$$Q_T[a] = \frac{1152}{103} g_{NL}^{(\partial\sigma)^4} \int_{-\infty}^0 d\tau_E \int_0^\infty dr r^2 \int d^2 \hat{\mathbf{n}} \left[\left(\sum_{\ell m} \nu_\ell(\tau_E, r) a_{\ell m} Y_{\ell m}(\hat{\mathbf{n}}) \right)^2 + \left| \sum_{\ell m} \omega_\ell(\tau_E, r) a_{\ell m} ({}_1 Y_{\ell m}(\hat{\mathbf{n}})) \right|^2 \right]^2 \quad (\text{C11})$$

4. Deviation from scale invariance

We have now obtained explicit factorizable representations for the shapes $\{g_{NL}^{\text{loc}}, g_{NL}^{\sigma^4}, g_{NL}^{(\partial\sigma)^4}\}$, but have assumed a scale invariant power spectrum $P_\zeta(k) = A_\zeta k^{-3}$ throughout. To compute these shapes in the WMAP or Planck cosmologies, we need to generalize slightly to the case of a power-law spectrum $P_\zeta(k) = A_\zeta k^{n_s-4}$.

In fact, our factorizable representations have been written in such a way that they generalize to an arbitrary power spectrum, by simply plugging it in whenever $P_\zeta(k)$ appears in the definitions (Eqs. (57), (61)) of the functions $\alpha_\ell(k)$, $\beta_\ell(k)$, $\mu_\ell(k)$, $\nu_\ell(\tau_E, k)$, and $\omega_\ell(\tau_E, k)$.

This prescription has several nice properties. First, it gives the correct trispectrum in the local case, i.e. when $\zeta = \zeta_G + g_{NL}^{\text{loc}} \zeta_G^3$ with arbitrary $P_\zeta(k)$. Second, it is the analogue of the prescription which is commonly used for the bispectrum (e.g. Eqs. (51)–(53) of [95]). Finally, for a power-law spectrum $P_\zeta(k) = A_\zeta k^{n_s-4}$, the ζ -trispectrum scales under dilations as:

$$\langle \zeta_{\lambda \mathbf{k}_1} \zeta_{\lambda \mathbf{k}_2} \zeta_{\lambda \mathbf{k}_3} \zeta_{\lambda \mathbf{k}_4} \rangle' = \lambda^{3(n_s-4)} \langle \zeta_{\mathbf{k}_1} \zeta_{\mathbf{k}_2} \zeta_{\mathbf{k}_3} \zeta_{\mathbf{k}_4} \rangle' \quad (\text{C12})$$

In the case of trispectra other than the local one, the deviation from scale invariance of the bispectrum and trispectrum cannot be reconstructed from the tilt of the power spectrum [96]. The above parametrization is however the closer guess to the actual dependence we can expect, and it is the correct one for the local case.

Appendix D: Numerical calculation of trispectra

We have now written down factorizable representations for the local, $\dot{\sigma}^4$, and $(\partial\sigma)^4$ trispectra. In this appendix we discuss computational issues in calculating these trispectra numerically. The chain of steps is:

1. We precompute the CMB transfer function $\Delta_\ell(k)$ on a grid of k -values.
2. Each trispectrum shape is represented either as a single integral over r (in the case of the local shape, Eq. (C2)) or double integral over (τ_E, r) (in the case of the $\dot{\sigma}^4$ and $(\partial\sigma)^4$ shapes, Eqs. (C5) and (C11)). We choose a finite sampling for this integral, in order to obtain a factorizable representation with a finite number of terms.
3. For each point in the (τ_E, r) plane, we compute the functions $\alpha_\ell(r)$, $\beta_\ell(r)$, $\mu_\ell(\tau_E, r)$, $\nu_\ell(\tau_E, r)$, and $\omega_\ell(\tau_E, r)$ appearing in the factorizable representation by evaluating the appropriate k -integral (Eqs. (57), (61)).

Let us consider each of these steps in detail, starting with the CMB transfer function $\Delta_\ell(k)$. The transfer function can be written as a line-of-sight integral [97]:

$$\Delta_\ell(k) = \int d\chi S(\chi, k) j_\ell(k\chi) \quad (D1)$$

We obtain the source function $S(\chi, k)$ from CAMB [83] and evaluate the above integral using equal spacing $\Delta\chi$. We compute the transfer function up to maximum wavenumber k_{\max} on a grid of k -values defined using the k -dependent step size $\Delta k = \min(\epsilon k, \kappa_0)$. This sampling scheme switches from equal spacing in $\log(k)$ at low- k to equal spacing in k at high- k . We choose the following default values for the parameters just defined:

$$(\Delta\chi, k_{\max}, \epsilon, \kappa_0) = (0.5, 5000r_{\text{horiz}}^{-1}, 2 \times 10^{-3}, 3 \times 10^{-5}) \quad (D2)$$

Next consider discretization of the (τ_E, r) integral (step 2 above). We discretize the outer τ_E integral using equally spaced points in $\log|\tau_E|$ from initial time τ_{Ei} to final time τ_{Ef} . Our default parameter values are:

$$(\tau_{Ei}, \tau_{Ef}, \Delta \log|\tau_E|) = \left(-10^6 \text{ Mpc}, -\frac{50 \text{ Mpc}}{\ell_{\max}}, \frac{\log(10)}{3} \right) \quad (D3)$$

For each τ_E , we discretize the inner r integral as follows. Let r_{rec} and r_{horiz} be the comoving distance to recombination and the causal horizon respectively. The integral formally goes to $r = \infty$, but the integrand decays beyond r_{horiz} , with characteristic decay scale given by $|\tau_E|$ plus the sound horizon. Therefore, we integrate from $r = 0$ to $r_{\max} = r_{\text{horiz}} + \rho_0 + \alpha|\tau_E|$, with default parameter values

$$(\rho_0, \alpha) = (2000 \text{ Mpc}, 10) \quad (D4)$$

We sample the r integral with spacing $(\Delta r)_1$ from $r = 0$ to r_{rec} , spacing $(\Delta r)_2$ from r_{rec} to r_{horiz} , and spacing $(\Delta r)_1$ from r_{horiz} to r_{\max} , where

$$(\Delta r)_1 = \max(\rho_1, \beta|\tau_E|) \quad (\Delta r)_2 = \max(\rho_2, \beta|\tau_E|) \quad (D5)$$

with default parameter values:

$$(\rho_1, \rho_2, \beta) = (50 \text{ Mpc}, 5 \text{ Mpc}, 0.1) \quad (D6)$$

In the case where the trispectrum is represented as a single integral over r , rather than a double integral over (τ_E, r) , we use the r -sampling for $\tau_E = 0$.

Finally, consider evaluation of k -integrals (step 3 above). We sample the integrals at the same values of k where the transfer function is computed as described previously. The k -integrals include factors of either the spherical Bessel function $j_\ell(x)$ or its derivative $j'_\ell(x)$. We precompute $j_\ell(x)$ using Steed's algorithm [98] on a regularly spaced grid with $\Delta x = 0.2$ and interpolate to arbitrary x . To evaluate $j'_\ell(x)$ we use the identity:

$$j'_\ell(x) = \frac{\ell}{2\ell+1} j_{\ell-1}(x) - \frac{\ell+1}{2\ell+1} j_{\ell+1}(x) \quad (\text{for } \ell \geq 1). \quad (D7)$$

This concludes our description of the numerics. To verify that numerical errors are fully controlled, we use the following end-to-end convergence test. In the above discussion we defined tolerance parameters controlling the accuracy of the integration. We compute an ‘‘improved’’ trispectrum using more conservative values of tolerance parameters as follows:

$$\begin{aligned} & (\tau_{Ei}, \tau_{Ef}, \Delta \log|\tau_E|, \rho_0, \rho_1, \rho_2, \beta, k_{\max}, \epsilon, \kappa_0, \Delta\chi, \Delta x) \\ & \rightarrow \left(-10\tau_{Ei}, -\frac{\tau_{Ef}}{10}, \frac{2}{3} \log|\tau_E|, 2\rho_0, \frac{\rho_1}{2}, \frac{\rho_2}{2}, \frac{\beta}{2}, 2k_{\max}, \frac{\epsilon}{2}, \frac{\kappa_0}{2}, \frac{\Delta\chi}{2}, \frac{\Delta x}{2} \right) \end{aligned} \quad (D8)$$

and also adjusting several parameters in CAMB. We then verify that the original and improved trispectra are nearly equal, in the metric defined by the Fisher matrix. For this comparison, we do not optimize the trispectra, since the number of terms N_{fact} in the improved trispectrum will be very large, and the optimization algorithm will be too slow, but computing the Fisher matrix is still affordable using the Monte Carlo algorithm from §VIA. This end-to-end test is a complete check that any numerical errors in our calculation of the trispectrum are not observationally important.

Appendix E: Constructing the estimator \hat{F}

In the optimal pipeline (§IX A) we introduced the following estimator:

$$\begin{aligned} \hat{F} = & \frac{\alpha}{2} \left\langle (\partial_{\ell m} Q[\tilde{b}, \tilde{b}, \tilde{b}]) C_{\ell m, \ell' m'}^{-1} (\partial_{\ell' m'} Q[\tilde{b}, \tilde{b}, \tilde{b}]) + (\partial_{\ell m} Q[\tilde{b}', \tilde{b}', \tilde{b}']) C_{\ell m, \ell' m'}^{-1} (\partial_{\ell' m'} Q[\tilde{b}', \tilde{b}', \tilde{b}']) \right\rangle \\ & + \frac{\beta}{2} \left\langle (\partial_{\ell m} Q[\tilde{b}, \tilde{b}, \tilde{b}']) C_{\ell m, \ell' m'}^{-1} (\partial_{\ell' m'} Q[\tilde{b}, \tilde{b}, \tilde{b}']) + (\partial_{\ell m} Q[\tilde{b}, \tilde{b}', \tilde{b}']) C_{\ell m, \ell' m'}^{-1} (\partial_{\ell' m'} Q[\tilde{b}, \tilde{b}', \tilde{b}']) \right\rangle \\ & + \frac{\gamma}{2} \left\langle (\partial_{\ell m} Q[\tilde{b}, \tilde{b}, \tilde{b}]) C_{\ell m, \ell' m'}^{-1} (\partial_{\ell' m'} Q[\tilde{b}, \tilde{b}', \tilde{b}']) + (\partial_{\ell m} Q[\tilde{b}', \tilde{b}', \tilde{b}']) C_{\ell m, \ell' m'}^{-1} (\partial_{\ell' m'} Q[\tilde{b}, \tilde{b}, \tilde{b}']) \right\rangle \end{aligned} \quad (\text{E1})$$

with coefficients $(\alpha, \beta, \gamma) = (1/16, 9/16, -3/8)$. In this appendix we explain how these coefficients were chosen.

We use a ‘‘contraction’’ notation in which each line between factors of T denotes one factor of $C_{\ell m, \ell' m'}^{-1}$ contracted with the appropriate indices. For example, the quantity F defined in Eq. (25) could be denoted:

$$F = \frac{1}{4!} \left(\overbrace{T \quad T}^{\overbrace{\quad\quad\quad}^{\overbrace{\quad\quad\quad}^{\overbrace{\quad\quad\quad}^{\quad\quad\quad}}} \right) = \frac{1}{4!} \sum_{\ell_i m_i \ell'_i m'_i} T_{m_1 m_2 m_3 m_4}^{\ell_1 \ell_2 \ell_3 \ell_4} C_{\ell_1 m_1, \ell'_1 m'_1}^{-1} C_{\ell_2 m_2, \ell'_2 m'_2}^{-1} C_{\ell_3 m_3, \ell'_3 m'_3}^{-1} C_{\ell_4 m_4, \ell'_4 m'_4}^{-1} T_{m'_1 m'_2 m'_3 m'_4}^{\ell'_1 \ell'_2 \ell'_3 \ell'_4} \quad (\text{E2})$$

and, as another example:

$$\left(\overbrace{T \quad T}^{\overbrace{\quad\quad\quad}^{\overbrace{\quad\quad\quad}^{\overbrace{\quad\quad\quad}^{\quad\quad\quad}}} \right) = \sum_{\ell_i m_i \ell'_i m'_i} T_{m_1 m'_1 m_3 m_4}^{\ell_1 \ell'_1 \ell_3 \ell_4} C_{\ell_1 m_1, \ell'_1 m'_1}^{-1} C_{\ell_2 m_2, \ell'_2 m'_2}^{-1} C_{\ell_3 m_3, \ell'_3 m'_3}^{-1} C_{\ell_4 m_4, \ell'_4 m'_4}^{-1} T_{m'_1 m'_2 m'_3 m'_4}^{\ell_2 \ell'_2 \ell_3 \ell'_3} \quad (\text{E3})$$

Our estimator \hat{F} should have the property that $\langle \hat{F} \rangle = F$. It is easy to calculate the expectation value of Eq. (E1), obtaining:

$$\langle \hat{F} \rangle = \left(\frac{\alpha}{6} + \frac{\beta}{18} \right) \left(\overbrace{T \quad T}^{\overbrace{\quad\quad\quad}^{\overbrace{\quad\quad\quad}^{\overbrace{\quad\quad\quad}^{\quad\quad\quad}}} \right) + \left(\frac{\alpha}{4} + \frac{\beta}{36} + \frac{\gamma}{12} \right) \left(\overbrace{T \quad T}^{\overbrace{\quad\quad\quad}^{\overbrace{\quad\quad\quad}^{\overbrace{\quad\quad\quad}^{\quad\quad\quad}}} \right) \quad (\text{E4})$$

We see that $\langle \hat{F} \rangle = F$ if the coefficients (α, β, γ) satisfy the constraints:

$$\frac{\alpha}{6} + \frac{\beta}{18} = \frac{1}{24} \quad \frac{\alpha}{4} + \frac{\beta}{36} + \frac{\gamma}{12} = 0 \quad (\text{E5})$$

These constraints do not fully determine (α, β, γ) ; there is a 1-parameter family of solutions. We noticed empirically that the choice $(\alpha, \beta, \gamma) = (1/16, 9/16, -3/8)$ nearly minimizes the variance $\text{Var}(\hat{F})$, and even a small change in these coefficients results in a dramatically larger value of $\text{Var}(\hat{F})$. We subsequently found a semianalytic explanation for this phenomenon as follows. The variance $\text{Var}(\hat{F})$ is a sixteen-point function which can be expanded using Wick’s theorem as a sum of many terms. One of these terms is:

$$\text{Var}(\hat{F}) \supset \left(12\alpha + \frac{4}{3}\beta + 4\gamma \right)^2 \left(\overbrace{T \quad T}^{\overbrace{\quad\quad\quad}^{\overbrace{\quad\quad\quad}^{\overbrace{\quad\quad\quad}^{\quad\quad\quad}}} \right) \left(\overbrace{T \quad T}^{\overbrace{\quad\quad\quad}^{\overbrace{\quad\quad\quad}^{\overbrace{\quad\quad\quad}^{\quad\quad\quad}}} \right) \quad (\text{E6})$$

We can speculate that this term will dominate $\text{Var}(\hat{F})$, since it ‘‘maximally factors’’ in the sense defined in [99]. If we set this term to zero by imposing the constraint $12\alpha + (4/3)\beta + 4\gamma = 0$ in addition to the constraints (E5), then we obtain the coefficients $(\alpha, \beta, \gamma) = (1/16, 9/16, -3/8)$.

Appendix F: Efficient evaluation of \hat{F}_V and $\text{Var}(\hat{F}_V)$

In the pure MC pipeline (§IX B), we gave expressions for estimators \hat{F}_V and $\hat{\Sigma}$, used to estimate the statistical error on g_{NL} , and the “error on the error”. As given (in Eqs. (90) and (91)), these expressions have computational cost $\mathcal{O}(N_{\text{mc}}^4)$ and $\mathcal{O}(N_{\text{mc}}^8)$ respectively. In this appendix we give mathematically equivalent expressions with cost $\mathcal{O}(N_{\text{mc}}^2)$ and $\mathcal{O}(N_{\text{mc}}^3)$.

We decompose $R_{ij} = S_{ij} + T_i + T_j + U$, where we have defined

$$U = \frac{\sum_{ij} R_{ij}}{N(N-1)} \quad T_i = \frac{\sum_j R_{ij}}{N-2} - \frac{\sum_{jk} R_{jk}}{N(N-2)} \quad S_{ij} = \begin{cases} R_{ij} - T_i - T_j - U & \text{if } i \neq j \\ 0 & \text{if } i = j \end{cases} \quad (\text{F1})$$

This is the unique decomposition $R_{ij} = S_{ij} + T_i + T_j + U$ (for $i \neq j$) satisfying $\sum_i T_i = \sum_i S_{ij} = S_{ii} = 0$. In terms of the new variables S, T, U , a long computer algebra assisted calculation gives the following alternate forms for \hat{F}_V and $\hat{\Sigma}$:

$$\begin{aligned} \hat{F}_V &= \frac{\sum_i T_i^2}{N-1} - \frac{\sum_{ij} S_{ij}^2}{N(N-2)(N-3)} \\ \hat{\Sigma} &= \left(\frac{(N-1)^2}{N_4^2} - \frac{N^2 - 9N + 26}{N_8} \right) \left(\sum_{ij} S_{ij}^2 \right)^2 + 6 \frac{N-3}{N_6} \left(\sum_{ij} S_{ij}^2 \right) \left(\sum_i T_i^2 \right) - \frac{N^2 - 3}{(N-1)N_4} \left(\sum_i T_i^2 \right)^2 \\ &\quad + \frac{13N^2 - 73N + 162}{N_8} \left(\sum_{ijk} S_{ij}^2 S_{jk}^2 \right) + 4 \frac{3N^2 - 7N - 2}{N_8} \left(\sum_{ijk} S_{ij}^2 S_{ik} S_{jk} \right) - 2 \frac{5N^2 - 17N + 18}{N_8} \left(\sum_{ij} S_{ij}^4 \right) \\ &\quad - 2 \frac{N^2 - 5N + 10}{N_8} \left(\sum_{ijkl} S_{ij} S_{jk} S_{kl} S_{il} \right) + 16 \frac{N(N-2)}{N_7} \left(\sum_{ij} S_{ij}^3 T_j \right) - 12 \frac{N^2 - 5N + 10}{N_7} \left(\sum_{ijk} S_{ij}^2 S_{jk} T_k \right) \\ &\quad - 8 \frac{N(N-2)}{N_7} \left(\sum_{ijk} S_{ij} S_{jk} S_{ik} T_k \right) + 4 \frac{N^2 - 4N + 7}{N_6} \left(\sum_{ijk} S_{ij} S_{jk} T_i T_k \right) - 2 \frac{5N^2 - 13N + 12}{N_6} \left(\sum_{ij} S_{ij}^2 T_j^2 \right) \\ &\quad - 4 \frac{(N+3)(N-2)}{N_6} \left(\sum_{ij} S_{ij}^2 T_i T_j \right) + 4 \frac{N(N-1)}{N_5} \left(\sum_{ij} S_{ij} T_i T_j^2 \right) + \frac{N(N-1)}{N_4} \left(\sum_i T_i^4 \right) \end{aligned} \quad (\text{F2})$$